LARGE-SCALE BIOLOGY ARTICLE

Advanced Cataloging of Lysine-63 Polyubiquitin Networks by Genomic, Interactome, and Sensor-based Proteomic Analyses

Natali Romero-Barrios[a], Dario Monachello[b,c], Ulla Dolde[d], Aloysius Wong[a], Hélène San Clemente[d], Anne Cayrel[a], Alexander Johnson[a], Claire Lurin[b,c], and Grégory Vert[a,d,1]

[a] Institute for Integrative Biology of the Cell (I2BC), CNRS/CEA/Univ. Paris Sud, Université Paris-Saclay, 91198 Gif-sur-Yvette, France.
[b] Institute of Plant Sciences Paris-Saclay (IPS2), CNRS, INRA, Université Paris-Sud, Université d'Evry, Université Paris-Saclay, 91405 0rsay, France
[c] Institute of plant Sciences Paris-Saclay (IPS2), CNRS, INRA Université Paris-Diderot, Sorbonne Paris-Cité, 91405 Orsay, France
[d] Plant Science Research Laboratory (LRSV), UMR5546 CNRS/Université Toulouse 3, 31320 Castanet-Tolosan, France.
[1] Corresponding Author: Gregory.vert@lrsv.ups-tlse.fr

Short title: K63 polyubiquitin networks in plants

One sentence summary: Comprehensive analysis of lysine-63 polyubiquitination sheds light on its importance to plant growth and development and identifies the machinery driving this post-translational modification.

The author responsible for distribution of materials integral to the findings presented in this article in accordance with the policy described in the Instructions for Authors (www.plantcell.org) is: Grégory Vert (Gregory.Vert@lrsv.ups-tlse.fr).

ABSTRACT

The lack of resolution when studying the many different ubiquitin chain types found in eukaryotic cells has been a major hurdle to our understanding of their specific roles. We currently have very little insight into the cellular and physiological functions of lysine(K)63-linked ubiquitin chains, although they are the second most abundant forms of ubiquitin in plant cells. To overcome this problem, we developed several large-scale approaches to characterize i) the E2-E3 ubiquitination machinery driving K63-linked ubiquitin chain formation, and ii) K63 polyubiquitination targets to provide a comprehensive picture of K63 polyubiquitin networks in *Arabidopsis thaliana*. Our work identified the ubiquitin-conjugating enzymes (E2s) UBC35/36 as the major drivers of K63 polyubiquitin chain formation and highlights the major role of these proteins in plant growth and development. Interactome approaches allowed us to identify many proteins that interact with the K63 polyubiquitination-dedicated E2s UBC35/36 and their cognate E2 variants, including over a dozen E3 ligases and their putative targets. In parallel, we improved the *in vivo* detection of proteins decorated with K63-linked ubiquitin chains by sensor-based proteomics, yielding important insights into the roles of K63 polyubiquitination in plant cells. This work strongly increases our understanding of K63 polyubiquitination networks and functions in plants.

INTRODUCTION

Post-translational modification of proteins by the 76-amino-acid polypeptide ubiquitin (Ub) is crucial for regulating protein stability, activity, localization, or interactions with partners

(Mukhopadhyay and Riezman, 2007). Ubiquitination involves the sequential action of three classes of enzymes: ubiquitin-activating enzymes (E1s), ubiquitin-conjugating enzymes (E2s), and ubiquitin ligases (E3s). The activities of these enzymes ultimately result in the covalent attachment of Ub to a lysine (K) residue in the target protein. Polyubiquitin (polyUb) chains are formed by the further attachment of Ub moieties linked together by one of the seven lysine residues present in a Ub molecule (K6, K11, K27, K29, K33, K48, and K63) or by the N-terminal methionine in the form of head-tail linear repeats (Peng et al., 2003; Pickart and Fushman, 2004; Kirisako et al., 2006). PolyUb chains exhibit different topologies and are associated with diverse biological functions (Woelk et al., 2007). K48-linkage of Ub moieties triggers the degradation of target proteins by the 26S proteasome (Pickart and Fushman, 2004). Much less is known about the other polyUb chain linkages (Pickart and Fushman, 2004; Kirisako et al., 2006; Woelk et al., 2007). K63-linked Ub chains do not induce proteasome-dependent degradation. The roles of polyubiquitination involving residue K63 from Ub (hereafter referred to as K63 polyubiquitination) have been widely studied in yeast and mammals, including roles in the endocytosis of plasma membrane proteins, DNA damage responses, and more marginally autophagy and signaling (Woelk et al., 2007; Adhikari and Chen, 2009; Komander and Rape, 2012).

Extensive work in non-plant model organisms has demonstrated that K63 polyUb chains form via two distinct mechanisms. First, HECT-type E3s have the ability to directly transfer Ub moieties to target proteins and thus catalyze the formation of specific linkage types regardless of the E2 (Kim and Huibregtse, 2009; Sheng et al., 2012). For non-HECT E3s, K63 polyUb is dictated by the E2 UBC13 (UBIQUITIN CONJUGATING ENZYME13) and involves a heterodimeric complex composed of UBC13 and the UEV1/MMS2 E2 variants (E2v), which lack the active-site cysteine residue. Mechanistically, K63 polyUb chain formation requires the active-site cysteine of UBC13 to be covalently bound to a first donor Ub, while UEV1/MMS2 binds non-covalently to a second acceptor Ub to make residue K63 of Ub available for chain elongation (Hodge et al., 2016). E2v also provide specificity to the UBC13-mediated K63 polyUb. In humans for example, the UBC13/MMS2 heterodimer drives K63 polyUb in the nucleus and DNA damage responses, while UBC13/UEV1A is involved in cytoplasmic K63-linked chain formation and drives NF-κB signaling, a crucial process controlling cytokine production, inflammation and immunity (Hofmann and Pickart, 1999, 2001; Andersen et al., 2005).

Plant genomes have a relatively low number of HECT E3s, with only 7 HECT E3s encoded in Arabidopsis among a total of 1500 E3s (Romero-Barrios and Vert, 2018). In comparison, humans possess 600 E3s with ~30 HECT E3 members. By contrast, Arabidopsis has more UBC13-type E2s and UEV1 E2v than humans, with two UBC13 E2s (UBC35/36) among the 37 Arabidopsis E2s and four UEV1 E2v (UEV1A-D). Similar to what has been described in humans, plant UEV1s confer specificity to K63 polyubiquitination events, with UEV1B and UEV1C primarily accumulating in the nucleus and UEV1A mostly accumulating in the cytosol in *Brachypodium distachyon* (Guo et al., 2016).

The characterization of *Arabidopsis thaliana* T-DNA mutant alleles of the K63 polyubiquitination machinery has shed light on its participation to several biological processes. The *ubc35-1 ubc36-1* and *uev1d* mutants both show hypersensitivity to DNA damaging agents (Wen et al., 2008; Pan and Schmidt, 2014), similar to their yeast and mammalian counterparts. The *ubc35-1* mutant is unable to form branched root hairs upon iron starvation and mis-expresses genes regulated by iron, pointing to a role of UBC35 in iron metabolism (Li and Schmidt, 2010). *ubc35-1 ubc36-1* also shows shorter primary roots, fewer lateral roots and root hairs, and lower sensitivity to exogenously applied auxin than the wild type (Wen et al., 2014). Finally, UBC13-type E2s from Arabidopsis and tomato (*Solanum lycopersicum*), or tomato UEV1s, have been connected to pathogen responses (Mural et al., 2013; Turek et al., 2018; Wang et al., 2019). Even though many pathways appear to be targeted by the loss of UBC35/36 or UEV1A-D, the rather mild developmental defects observed in the corresponding loss-of-function mutants argue either for a non-essential role of K63 polyubiquitination in plants or to the prominent role of HECT-type E3s in the global landscape of K63 polyubiquitination despite their low number.

Until recently, only a few plant proteins were reported to be K63 polyubiquitinated, although K63 polyubiquitination represents the second most abundant ubiquitination type after K48-linked chains (Kim et al., 2013). In most cases, these are membrane proteins for which K63 polyubiquitination drives their endocytosis and degradation in the vacuole (Romero-Barrios and Vert, 2018). Advanced mass spectrometry approaches using TUBE-based affinity purification of ubiquitinated proteins or using TUBE or COmbined FRActional DIagonal Chromatography (COFRADIC) identified thousands of ubiquitinated proteins and ubiquitin attachment sites within (Kim et al., 2013; Walton et al., 2016b). However, both strategies fail to provide information on Ub linkages, limiting our ability to tackle the roles of K63 polyUb

chains with precision. Using a K63 polyUb sensor based on yeast VPS27 that recognizes K63-linked Ub chains (Sims et al., 2012; van Wijk et al., 2012), we recently identified ~100 Arabidopsis proteins as part of the first plant K63 polyubiquitome (Johnson and Vert, 2016). This analysis revealed a tight link between K63 polyubiquitination and membrane proteins, likely underlying their degradation through endocytosis. Another striking connection was established with ribosomal proteins, which is consistent with the reported role of K63 polyubiquitination in sustaining translation efficiency under stress conditions in yeast (Silva et al., 2015; Back et al., 2019). Therefore, such a powerful sensor-based proteomic approach provided the first glimpse of the K63 polyubiquitination networks in plants and has the great potential to uncover unsuspected roles of this still poorly characterized post-translational modification. Here, to increase our resolution of K63 polyubiquitination networks, we conducted several complementary large-scale approaches to probe the composition and functional importance of the K63 polyubiquitination machinery as well as its targets in Arabidopsis. This analysis allowed us not only to provide a better picture of K63 polyubiquitination-dependent processes in plants, but also to identify roles of K63 polyubiquitination in various processes such as nuclear import, splicing, and DNA structure/topology.

RESULTS

K63 polyubiquitination catalyzed by UBC35/36 is essential for plant growth and development

To functionally characterize the importance of K63 polyubiquitination and evaluate the contribution of UBC13 homologs to the formation of K63 polyUb chains in plants, we isolated T-DNA knock-out alleles for the two Arabidopsis *UBC13* genes *UBC35* and *UBC36* (Supplemental Figure 1A). The *ubc35-1* allele (WiscDsLox323H12) harbored no mRNA for *UBC35* and is therefore a null mutant (Supplemental Figure 1B), which is consistent with previous reports (Li and Schmidt, 2010; Wen et al., 2014). By contrast, the *ubc36-1* allele (SALK_047381) still showed *UBC36* mRNA accumulation albeit to a lesser extent than its wild-type counterpart (Supplemental Figure 1B). Although the same *ubc36-1* allele was previously reported to be a knock-out (Wen et al., 2014), we obtained evidence that *ubc36-1* is a knock-down allele. Regardless, both *ubc35-1* and *ubc36-1* showed no macroscopic phenotype (Supplemental Figure 1C). We also confirmed that the *ubc35-1 ubc36-1* double mutant still accumulated *UBC36* mRNA (Supplemental Figure 1D).

To examine the consequences of loss-of-function of *UBC13* in plants, we isolated a new *ubc36* knock-out allele (GABI_836B11) showing no *UBC36* mRNA accumulation (Supplemental Figure 1A, Figure 1A), which we named *ubc36-2*. Similar to *ubc35-1*, *ubc36-2* showed no macroscopic phenotype despite being impaired in the accumulation of K63 polyubiquitinated proteins (Figure 1B, 1C). The drop in K63 polyubiquitinated protein accumulation observed in both mutants supports the idea that Arabidopsis E2 enzymes UBC35 and UBC36 are the functional homologs of UBC13 from yeast and act redundantly to catalyze the formation of K63 polyUb chains. To evaluate the functional consequences of a total loss of UBC13-dependent K63 polyubiquitination in plants, we crossed *ubc35-1* and *ubc36-2* plants. In contrast to *ubc35-1 ubc36-1*, the *ubc35-1 ubc36-2* double mutant completely lacked *UBC35* and *UBC36* transcripts (Figure 1A). Very strong growth defects were observed for homozygous *ubc35-1 ubc36-2* mutants, with most plants arresting after germination. The penetrance of the mutations was not complete, since ~5% of homozygous *ubc35-1 ubc36-2* plants developed to the point of producing a few seeds but were devoid of detectable K63 polyubiquitinated proteins (Figure 1B, 1D, 1E). F3 seeds germinated poorly and never developed beyond the cotyledon stage, further pointing to the major role of UBC13-type E2s (Figure 1F). These phenotypes are overall much more dramatic than the previously reported phenotypes of *ubc35-1 ubc36-1* plants (Li and Schmidt, 2010; Wen et al., 2014), which is consistent with the finding that *ubc36-1* used in these published studies is not a null allele. The severity of the growth defects of *ubc35-1 ubc36-2* is also in accordance with the finding that plants expressing ubiquitination-defective forms of proteins known to be modified with K63 polyUb chains, such as the metal transporter IRT1, are strongly impaired (Barberon et al., 2011; Dubeaux et al., 2018). Altogether, our work sheds light on the crucial roles of UBC13-type E2s and K63 polyUb chain formation in plant growth and development.

Genomic responses dependent on K63 polyUb chain formation

To pinpoint the cellular or physiological functions that are dependent on the formation of K63 polyUb chains, we sought to characterize the genomic responses to the loss of UBC13-type of E2s. Considering the extreme severity of the *ubc35-1 ubc36-2* double mutant phenotype, we generated transgenic lines expressing an artificial microRNA targeting both *UBC35* and *UBC36* (amiUBC35/36) under the control of an estradiol-inducible promoter. amiUBC35/36-expressing lines grown on β-estradiol-containing plates showed a robust decrease in UBC13 protein accumulation (Figure 2A). Downregulation of *UBC35*/*36* expression resulted in reduced root growth (Figure 2B), similar to what has been observed in *ubc35-1 ubc36-1*

plants and consistent with the finding that amiUBC35/36 plants still possess ~25% of wild-type levels of total UBC13-type E2s. To evaluate the global changes associated with the downregulation of *UBC35*/*36*, we performed RNA-seq analysis of mock-treated and estradiol-induced amiUBC35/36 lines. A profound genomic reprogramming occurred upon downregulation of *UBC35* and *UBC36* gene expression, with ~700 of genes upregulated and ~1000 genes downregulated (p-value <0.01, fold change >1.5) (Figure 2C; Supplemental Data Set 1, 2). Gene Ontology (GO) enrichment analysis indicated that upregulated genes in the amiUBC35/36 lines were significantly enriched in GO terms response to abiotic (light, oxidative stress, nutrition, heat) and biotic (oomycetes, insects and fungi) stresses, while terms corresponding to RNA processing were underrepresented (Supplemental Data Set 3). GO terms corresponding to glucosinolate biosynthesis, cell cycle, microtubule-based processes, and RNA processing were either over- or under-represented among downregulated genes (Supplemental Data Set 4). Therefore, the biological processes associated with these terms represent putative cellular functions requiring K63 polyubiquitination involving target proteins yet to be identified. Taken together, the genomic perturbations associated with impairment in the formation of K63 polyUb chains target multiple environmental stress responses as well as endogenous cellular functions, further pointing to the essential role of K63 polyUb in plant growth, development, and responses to the environment.

Interactome-based approach to study K63 polyUb networks

Having established that K63 polyUb chain formation requires both UBC35/36 E2s and participates in a wide variety of processes, we sought to identify E3 Ub ligases that interact with UBC35 and UBC36. This information is instrumental to better understand the biological roles associated with K63 polyubiquitination. We previously investigated the yeast two-hybrid (Y2H) first generation Arabidopsis interactome map AI-1, generated using a library of ~8,000 Arabidopsis open reading frames (ORFs) (8k_space), for proteins that interact with UBC36 and UEV1A, UEV1C or UEV1D (UBC35 and UEV1B were not present in the original 8k_space) (Arabidopsis Interactome Mapping, 2011). This study identified six E3 ligases among a total of 13 primary interacting proteins (Johnson and Vert, 2016). To extend the analysis of K63 polyUb networks, we determined protein-protein interactions between UBC35/36 and UEV1A-D (used as bait) and 12,000 Arabidopsis proteins encoded by sequence-verified ORFs (12k_space, InterAtome) in the Y2H mapping liquid pipeline (Monachello et al., 2019). Such screening of bait proteins against individual ORFs indeed allows the detection of weakly interacting proteins or proteins with low abundance that would

be masked in library-based yeast two-hybrid approaches. The complete ORF library encodes close to 50% of the Arabidopsis proteome and contains hundreds of factors belonging to the ubiquitination machinery, including ~450 E3 ligases (Supplemental Table 1). This data set allowed us to identify 24 protein-protein interactions (PPI) (Figure 3A; Supplemental Data Set 5). The complete list of interactions and annotations can be used to build networks with Cytoscape and to extract relevant information about K63 polyUb networks and subnetworks reported in the present study (Supplemental Data Set 6). Both UBC35 and UBC36 interacted with the four E2v UEV1A-D (Figure 3B; Supplemental Data Set 6). These E2v were previously shown to interact with UBC36 (Wen et al., 2008), thereby validating our interactome. Most of the PPIs identified in the original interactome for UBC/UEV1 were also picked up in our new interactome (11 out of 13; Figure 3C; Supplemental Data Set 5) (Johnson and Vert, 2016), but we have now uncovered 13 new PPIs for UBC35/36 and UEV1A-D. Overall, 13 E3 Ub ligases, mostly from the RING/U-box family, have been identified. These proteins are therefore likely involved in the selection of substrates to be modified with K63 polyUb chains. Two other proteins related to Ub and protein degradation but not belonging to the E3 ligase category were isolated, the COP9 signalosome subunit CSN5A and the Otubain-like deubiquitinase. Overall, analysis of the combination of the 12,000 and the 8,000 previously published ORF data sets, together with literature-curated interactions, yielded 28 PPIs for the UBC13-based K63 polyubiquitination machinery, with 13 E3 ligases potentially involved in substrate decoration with K63-linked Ub chains (Supplemental Data Set 7).

Further screening of the ORF library using primary interactants of UBC35/36 and UEV1A-D identified many secondary interacting proteins (Supplemental Figure 2, Supplemental Data Set 6). Considering that a few proteins act as major hubs and gather hundreds of interactions each, we removed such hubs to better highlight the network of interactions (Figure 4A). Of particular interest is the identification of several partners of UBC35/36-UEV1A-D-interacting E3s, which presumably represent E3 targets undergoing K63 polyubiquitination. As an example of E2-E3-target reconstitution, the RING E3 ligase encoded by the At5g38895 gene interacts with UBC35, UBC36 as well as with UEV1C and UEV1D, and also partners with the bHLH transcription factor HEC2 (Figure 4B). HEC proteins are known to control the female reproductive tract, shoot apical meristem development and photomorphogenesis in Arabidopsis (Gremski et al., 2007; Schuster et al., 2015). Our interactome analyses suggest that HEC2-dependent functions in plant development may be regulated by K63

polyubiquitination. Overall, the interactome-based characterization presented here yields important perspective into the biological functions of K63 polyubiquitination by identifying molecular actors at stake in pathways and responses shown to require this post-translational modification.

Identification of K63 polyubiquitinated proteins by sensor-based proteomics

To obtain more direct insights into K63 polyubiquitination, we continued our effort to catalog proteins decorated with K63 polyUb chains *in vivo*. Using a K63 polyUb-specific sensor to immunopurify proteins modified with K63-linked polyUb chains, we previously isolated ~100 proteins as part of the K63 polyubiquitome in plants (Johnson and Vert, 2016). To provide a deeper coverage of K63 polyubiquitinated proteins *in vivo*, we took two complementary approaches in this study. The first strategy was to use a longer column and longer gradient to improve peptide separation during chromatography, thus increasing resolution. The second approach took advantage of transgenic lines expressing a modified version of the K63 polyUb sensor. The original Vx3K0-GFP sensor line shows a mostly cytosolic localization, with enrichment in the plasma membrane and endosomes, but this sensor is globally excluded from the nucleus in Arabidopsis plants (Johnson and Vert, 2016). However, we now know that UBC35 and UBC36, the major determinants of K63 polyUb chain formation, localize to both the cytosol and nucleus (Supplemental Figure 3A-C). We therefore created a sensor that is also able to reach the nucleus thanks to the fusion with a nuclear localization signal (Vx3K0-NLS-mCit), together with its non-binding control (Vx3NB-NLS-mCit). We screened the mono-insertional homozygous transgenic lines for Vx3K0-NLS-mCit and Vx3NB-NLS-mCit based on their expression levels (Figure 5A). Consistent with a previous report, the point mutations introduced in Vx3NB created a mobility shift compared to Vx3K0 (Johnson and Vert, 2016). Care was taken to select lines showing low expression levels for Vx3K0-NLS-mCit to avoid detrimental effects of competing with endogenous K63 polyUb-binding proteins (Figure 5B).

Observation of the selected transgenic lines by confocal microscopy indicated that the Vx3NB-NLS non-binding control sensor localized exclusively to the nucleus (Figure 5C). By contrast, the Vx3K0-NLS binding sensor accumulated in the nucleus and cytosol, likely due to partial retention to cytosolic K63 polyubiquitinated proteins immediately after translation (Figure 5D). Vx3K0-NLS was also enriched in dotted structures, which were similar to the FM4-64-positive endosomes observed in Vx3K0-mCit lines (Johnson and Vert, 2016), as well

as in nuclear foci. These locations are consistent with the tight connection we and others previously uncovered between K63 polyubiquitination and membrane protein dynamics (Romero-Barrios and Vert, 2018). To decipher the biological relevance of such Vx3K0-NLS-positive nuclear foci, we evaluated the possible colocalization of known proteins marking nuclear foci (Lorkovic et al., 2008; Raczynska et al., 2014). Vx3K0-NLS-mCit did not co-localize significantly with the general splicing factor SR34-RFP (SERINE/ARGININE-RICH PROTEIN SPLICING FACTOR34) in nuclei (Pearson's correlation coefficient = 0.34; Figure 5E; Supplemental Figure 4A). However, extensive overlap with the HcRed-SERRATE protein was observed in nuclear foci (Pearson's correlation coefficient = 0.88; Figure 5F; Supplemental Figure 4B); this protein plays pivotal roles in various aspects of RNA metabolism, including microRNA biogenesis, constitutive and alternative splicing, biogenesis of non-coding RNAs, and RNA transport and stability. These findings again point to the likely requirement for K63 polyUb-decorated proteins in nuclear processes involving RNA processing.

To specifically isolate proteins carrying K63 polyUb chains *in vivo* and to eliminate possible co-purified proteins, we prepared total extracts from Vx3K0-NLS-mCit and Vx3NB-NLS-mCit seedlings using the stringent RIPA buffer, as previously described (Johnson and Vert, 2016). Vx3K0-NLS and Vx3NB-NLS were successfully immunoprecipitated using GFP-coupled microbeads (Supplemental Figure 5). K63 polyUb-decorated proteins were specifically recognized by Vx3K0-NLS, as visualized by probing immunoprecipitates with Apu3 antibodies (Figure 6A). The Ub sensor protected ubiquitinated proteins from deubiquitination in the cell and during the extraction process, as previously observed (Hjerpe et al., 2009; Johnson and Vert, 2016), allowing proteins carrying K63 polyubiquitin chains to accumulate in the input fraction (Figure 6A). To identify the proteins bound by Vx3K0-NLS-mCit, we subjected the immunoprecipitates to electrophoretic separation and Coomassie blue staining (Figure 6B, Supplemental Figure 6), followed by in-gel trypsin digestion and mass spectrometry analyses. A protein was considered for the K63 polyUb proteome catalog if two or more different matching peptides with protein and peptide thresholds of 95% or more were identified in Vx3K0-NLS data sets and absent from the negative control. Using these criteria and after eliminating contaminants, we identified close to 400 Arabidopsis proteins as potentially K63 polyubiquitinated (Supplemental Data Set 8), strongly increasing our resolution in identifying K63 polyubiquitination.

The recently established TUBE/USU and COFRADIC ubiquitomes serves as the reference list of ubiquitinated proteins (Kim et al., 2013; Walton et al., 2016a), although these studies provide no hint about the possible Ub linkages. Among the K63 polyubiquitome, 87 and 56 proteins were already identified as ubiquitinated in the TUBE/USU and COFRADIC proteomes, respectively (Figure 6C). Approximately 50 proteins are also common to the Vx3K0-NLS and Vx3K0 data sets, including many plasma membrane proteins (ATPases, transporters, channels). GO enrichment analysis of the Vx3K0-NLS ubiquitome revealed an over-representation of GO terms that overlapped with our previous Vx3K0 data set, such as GO terms related to metabolism, vesicular trafficking, and transport across membranes (Figure 6D, Supplemental Data Set 9). More interesting is the finding that, using the Vx3K0-NLS sensor, we identified many nuclear proteins that were not identified in our first K63 polyubiquitome (Table 1, Supplemental Data Set 10). GO annotations of the nuclear K63 polyubiquitome revealed enrichment of terms corresponding to nuclear structure, nuclear import/export, chromosome organization, or splicing (Supplemental Data Set 11). In particular, we identified several proteins linked to RNA binding, unwinding, or splicing, which is consistent with the enrichment of Vx3K0-NLS in SERRATE-positive nuclear foci. The nuclear import machinery also appears to be under the control of K63 polyubiquitination, with several nuclear pore complex and factors involved in nuclear cargo recognition and transport (importins, RAN GTPase Activated Protein). Proteins involved in nuclear positioning and the maintenance of nuclear shape, such as SUN1 (SAD1/UNC-84 DOMAIN PROTEIN1), SUN2, LINC1 (LITTLE NUCLEI1), and LINC4, were also found, raising the question about the role of K63 polyubiquitination in these processes. Finally, several histones were found to be K63 polyubiquitinated, including HISTONE VARIANT H2AX, for which K63 polyubiquitination has been tightly linked to DNA damage responses in yeast and mammals (Mattiroli et al., 2012). Overall, these findings demonstrate our ability to better detect K63 polyubiquitinated proteins using Vx3K0-NLS-based proteomics and our improved peptide separation setup, providing excellent resolution of K63 polyUb-dependent processes in plants.

Validation of nuclear targets of K63 polyubiquitination

Since the proteins included in the K63 polyubiquitome were identified based on their ability to be recognized by the Vx3K0-NLS K63 polyUb chain sensor, we decided to confirm the presence of K63 polyUb chains on these proteins using another approach. We first used SUN1 and H2AX as a test case. We expressed SUN1 and H2AX in stable Arabidopsis transgenic

lines as GFP fusions, extracted the fusion proteins using RIPA buffer amended with DUB inhibitors, and subjected them to immunoprecipitation using GFP antibodies coupled to magnetic microbeads. We probed the immunoprecipitates with GFP antibodies to confirm immunoprecipitation of the protein of interest and with Apu3 antibodies that specifically recognize K63 polyUb chains. The free GFP negative control showed no signal using Apu3, greatly contrasting with the typical high molecular weight smear observed for SUN1 and H2AX (Figure 7A, B). This result confirms that both proteins are indeed decorated with K63-linked Ub chains *in planta* and validates our K63 polyubiquitome. As an alternative method for rapidly validating our mass spectrometry data, we also tested the transient expression of SUN2, MEE5 (MATERNAL EFFECT EMBRYO ARREST5), and the histone H2B in wild tobacco (*Nicotiana benthamiana*) leaves. All three proteins showed nuclear localization, with SUN2 localized to the nuclear envelope, MEE5 to the nucleoplasm, and H2B to the nucleolus as well as in nuclear foci (Figure 8A, C, E). While the free GFP control yielded no signal upon detection with Apu3 antibodies, all three immunoprecipitated proteins showed a high molecular weight smear (Figure 8B, D, F), confirming that these proteins are K63 polyubiquitinated *in vivo*.

DISCUSSION

The existence of many possible polyubiquitination linkages remains a hurdle in the analysis of the biological roles of Ub (Komander and Rape, 2012). Only recently have scientists started to tackle the functions of subtypes of Ub modifications using antibodies or sensors able to recognize specific linkages, or deubiquitinase able to trim certain chains. In the present work, we developed several large-scale approaches to provide a better understanding of K63 polyUb-dependent processes and the corresponding machinery.

Detailed genetic, biochemical, and structural analyses in yeast and humans demonstrated that K63 polyUb chain formation is under the control of the UBC13-type E2s and their UEV1 E2v partners (Hodge et al., 2016). By interacting with E3s that select specific substrates to be modified, UBC13-type E2s and E2v directly transfer Ub moieties to target proteins as K63 polyUb chains. Besides UBC13/UEV1, HECT E3s also have the ability to catalyze K63 polyUb chain formation independently of E2s (Kim and Huibregtse, 2009; Sheng et al., 2012). However, the contribution of UBC13-type E2s to K63 polyUb chain formation was previously thought to be rather modest considering the mild developmental defects (reduced root hair number and bifurcation in response to low iron levels) and altered responses to low

iron levels, cold, pathogens, and auxin shown by UBC13-type E2 mutants (Li and Schmidt, 2010; Wen et al., 2014; Wang et al., 2019). Here, we demonstrated that *ubc36-1* is only a knock-down allele, preventing the assessment of the true contribution of UBC13-type E2s. Using a new *ubc36-2* null allele, we now show that UBC35 and UBC36 are absolutely essential for producing K63-linked polyUb chains in plants and are crucial for plant growth and development. This translates into the altered expression of hundreds of genes involved in the cell cycle, metabolism, and RNA- or microtubule-based processes, consequently affecting biotic and abiotic stress responses upon the loss of K63 polyUb chain formation. Such a prominent role of UBC35/36 also suggests that HECT-type E3s, only seven of which have been found in Arabidopsis, have much more limited and likely specialized functions in the K63 polyubiquitination of a few targets.

UBC13-type E2s act in concert with E3s that are responsible for the recruitment of substrate(s) to be K63 polyubiquitinated. Considering the vast number of E3s encoded by plants genomes, deciphering the identity of E3s that select substrates destined to be K63 polyUb-decorated has been a challenge. To address this issue, we searched for proteins able to interact with UBC35/36 as well as their E2v UEV1A-D and identified over a dozen Arabidopsis E3s likely involved in K63 polyubiquitination. This compares to the limited number of E3s that have been shown to target proteins for K63-linked ubiquitination in humans, with the best examples being RNF8, RNF168, Mdm2, TRAF6, cIAP1/2, CHIP, Parkin, UCHL1, TRAF2, and ITCH, together with the HECT E3s HectH9 and NEDD4-2 (Adhikary et al., 2005; Bertrand et al., 2008; Lim and Lim, 2011; Mattiroli et al., 2012). Most of the Arabidopsis E3s uncovered as UBC35/36 or UEV1A-D interactors are RING/U-Box E3 ligases, with the exception of a BTB-POZ E3 ligase. These findings support the conclusions of previous studies on E2-E3 pairing, revealing interactions between UBC35 and UBC36 with RING and plant U-box E3s (Kraft et al., 2005; Turek et al., 2018).

Surprisingly, no F-box proteins were found to interact with the K63 polyUb E2 machinery, although hundreds are present in the ORF library. This may be explained by the limited capacity of yeast two-hybrid analysis to detect interactions between UBC35/36 or UEV1A-D and factors from multi-subunit E3 ligases. However, since no interaction was observed between UBC35/36 or UEV1A-D and the E2-interacting subunit RBX1 from F-box-containing Cullin-RING E3 ligase CRL1 complexes either, we believe that instead, F-box proteins rarely engage in substrate selection for K63 polyubiquitination. Another important

finding is that UBC35 and UBC36 essentially interact with the same E3s, indicating that there is no sub-functionalization of these E2s. Global analysis of the ability of Arabidopsis E2s to interact with a subset of RING E3s already suggested that both UBC35 and UBC36 bind *in vitro* to the same RING members (Kraft et al., 2005), which is consistent with our current findings. Instead, UEV1 proteins have undergone diversification and specialization in both humans and plants. MMS2 drives UBC13-dependent K63 polyUb in the nucleus and DNA damage responses, while UEV1A is involved in cytoplasmic K63-linked chain formation and drives NFκB signaling (Hofmann and Pickart, 1999, 2001; Andersen et al., 2005). Similarly, in *B. distachyon*, UEV1B and UEV1C primarily accumulate in the nucleus, while UEV1A mostly accumulates in the cytosol (Guo et al., 2016).

Besides UBC35/36/UEV1A-D/E3 pairing, crucial information when studying ubiquitination processes includes the identities of E3 targets. By reiterating the screening of the 12k_space ORFs with UBC35/36- or UEV1A-D-interacting E3s, we identified many putative substrates of the K63 polyubiquitination machinery. This allowed us to reconstitute several E2/E2v-E3-target cascades. In addition to such cascades, our interactome also shed light on possible regulators of UBC35/36/UEV1A-D-interacting E3s, which possibly function in a K63 polyUb-independent manner. For example, the RING protein encoded by the At1g74370 gene interacts with UBC35/UBC36, with itself, and with another RING E3 ligase (At2g29270) (Figure 4C). The latter E3 may either be regulated by K63 polyubiquitination catalyzed by the UBC35/36-$RING_{At1g74370}$ machinery, or may instead be a direct regulator of $RING_{At1g74370}$ independently of K63 polyUb chain formation. Globally, validation of the presence of K63 polyUb chains on possible E3 targets is necessary to discriminate between these two scenarios. Regardless, the interactome-based characterization of UBC35/36/UEV1A-D performed in this study provided crucial insights into K63 polyubiquitination networks.

While our work provided a high-resolution snapshot of the K63 polyubiquitination machinery, there are still several limitations that need to be addressed to broaden our view of K63 polyUb networks. 1) Although well-suited to pick up interactions between UBC35/36 or UEV1A-D with E3s and their targets, our yeast-two hybrid interactome is restricted to the 12,000 ORFs available. Approximately two-thirds of plant E3s and half of the Arabidopsis proteome remain to be tested, which may reveal additional participants in K63 polyUb formation. 2) Yeast two-hybrid analysis is not the most appropriate approach for probing interactions with membrane-bound or organelle-localized (with the exception of the nucleus)

proteins, thereby providing a restricted view on K63 polyUb networks. 3) The identification of non-E3 proteins as interacting with UBC35/36 or UEV1A-D is puzzling, as these proteins are devoid of typical E2-interacting domains such as RING or U-box domains. These hits may therefore represent indirect interactions bridged by endogenous yeast proteins, for example. Alternatively, these non-E3 hits may use uncharacterized domains to interact with UBC35/36 or UEV1A-D and may therefore be genuine regulators of E2s. A good example is the Otubain-like thioesterase, which interacts with UBC36 and whose OTUB1 human counterpart binds to UBC13 and Ub and inhibits UBC13 catalytic activity (Nakada et al., 2010). 4) Some E3s have the ability to interact with several E2s, thereby recruiting targets to be decorated with different chain types. For example, human Mdm2, RNF8, and cIAP1/2 can trigger both K63- and K48-linked polyubiquitination, while TRAF6 and RNF168 are the only two known E3s that selectively target substrate proteins for K63-linked polyubiquitination (Wang et al., 2012). One should therefore keep in mind that targets identified in our interactome may not represent genuine K63 polyubiquitination targets but may instead be modified with other linkage types. The ability to detect K63 polyubiquitination of targets *in planta* consequently appears to an essential step for validation.

Using an improved Vx3K0-based sensor and mass spectrometry workflow, we have greatly increased the repertoire of Arabidopsis proteins known to be decorated with K63 polyUb chains *in vivo*. Although K63 polyUb-modified proteins were greatly enriched in our pipeline, a very large majority of peptides resulting from their tryptic digestion do not carry Ub footprints, which renders the detection of modified peptides difficult, as already reported (Johnson and Vert, 2016). Enriching Vx3K0-NLS-purified proteins for ubiquitinated peptides using K-ε-GG antibodies, which recognize Ub remnants after trypsin digestion (Kim et al., 2011; Udeshi et al., 2013), should strongly improve the detection of K63 polyubiquitination sites. Regardless, our current study reveals a strong connection between K63 polyubiquitination and processes such as the dynamics of organelles and endomembrane (fission of mitochondria, vesicular trafficking), the organization of the nucleus (nuclear envelope, DNA topology, microtubules, transcription), and photosynthesis.

Although global themes clearly emerged from our RNA-seq interactome, and proteomic analysis of the global functions dependent on K63 polyubiquitination, there is very limited overlap between the different data sets. This finding is expected for RNA-seq, which does not monitor K63 polyubiquitination *per se* but rather identifies genes whose expression is directly

or indirectly modulated by K63 polyubiquitination. The comparison of our proteomic and interactome data sets yielded 16 common proteins. While this analysis provided invaluable information about the entire cascade required to K63 polyubiquitinate these proteins, the overlap overall appears quite restricted. However, mass spectrometry and yeast two-hybrid approaches are known to generate largely non-overlapping candidate lists (Gavin et al., 2002) due to inherent differences in the processes monitored. For example, interactions involving membrane proteins cannot be probed in our yeast two-hybrid interactome. Both approaches, combined with the analysis of amiUBC35/36 transcriptomes, should therefore be considered complementary methods for establishing K63 polyubiquitination networks.

Altogether, the mapping of K63-linked Ub networks greatly increases our understanding of Ub in plants and highlights the contributions of K63 polyubiquitin to a wide array of cellular and physiological functions.

METHODS

Plant materials and growth conditions

Single *Arabidopsis thaliana ubc35-1* (WiscDsLox323H12) and *ubc36-1* (SALK_047381) mutants were described in a previous study (Li and Schmidt, 2010). *ubc36-2* (GABI_836B11) was obtained from NASC and genotyped to isolate homozygous mutants. *ubc35-1 ubc36-2* was obtained after crossing, selfing, and genotyping F2 plants.

Wild-type, *ubc35-1*, *ubc36-1*, *ubc36-2*, *ubc35-1 ubc36-1, ubc35-1 ubc36-2* plants and the transgenic lines 35S:UBC35-GFP, 35S:UBC36-GFP, Ubi10:Vx3K0-NLS-mCit, Ubi10:Vx3NB-NLS-mCit, Ubi10:GFP, Ubi10:H2AX-GFP, and Ubi10:H2B.11-GFP were grown under sterile conditions on vertical plates containing half-strength Linsmaier and Skoog medium at 21 °C. Plants were cultivated under a 16-h light/8h dark cycle with a light intensity of 90 μmole $\mu mol \cdot m^{-2} \cdot s^{-1}$ using Philips 17W F17T8/TL741 bulbs. Plants were grown in soil to obtain progeny or to assess macroscopic phenotypes.

Constructs

ORFs corresponding to *UBC35* and *UEV1B* were amplified and cloned into the pDONR207 vector by Gateway cloning using primers listed in Supplemental Data Set 12. LR recombinations were performed using the pDEST-AD-CYH2 and pDEST-DB destination

vectors, allowing N-terminal fusions with the activation domain (AD) or the DNA-binding (DB) of the GAL4 transcription factor (Dreze et al., 2010). Other baits (UBC36, UEV1A, UEV1C, UEV1D) were retrieved from the destination vectors derived from the Arabidopsis Interactome (Arabidopsis Interactome, 2011).

Vx3K0 and Vx3NB were a kind gift of Robert Cohen (Colorado State University, Fort Collins, CO, USA). The *Vx3K0* and *Vx3NB* cassettes, and *UBC35*, *UBC36*, *H2AX*, and *H2B.11* cDNAs were amplified by PCR with primers containing *att*B1 and *att*B2 Gateway recombination sites (Supplemental Data Set 12), and cloned into pDONR-P1P2. Expression vectors were constructed by multisite Gateway recombination of the pB7m34GW destination vector with pDONR-P4P1r-pUbi10 or pDONR-P4P1r-p35S for promoters, pDONR-P1P2-UBC35, pDONR-P1P2-UBC36, pDONR-P1P2-Vx3K0, pDONR-P1P2-Vx3NB, pDONR-P1P2-GFP, pDONR-P1P2-H2AX and pDONR-P1P2-H2B.11 for genes of interest, and pDONR-P2rP3-NLS-mCitrine for fluorescent reporters. *MEE5* (At1g06220) was amplified by PCR and cloned at the *Sma*I site under the control of the 35S promoter in the pPZP212-derived pCH3-GFP vector. SUN1:SUN1-GFP or SUN2:SUN2-GFP binary vectors were kindly provided by Katja Graumann (Oxford Brookes University, Oxford, England). Constructs for the generation of artificial microRNAs targeting UBC35 and UBC36 were prepared as described (http://wmd3.weigelworld.org/cgi-bin/webapp.cgi) using primers listed in Supplemental Data Set 12.

Stable transgenic lines were generated by the floral dip method (Clough and Bent, 1998). For each construct, several independent mono-insertional homozygous T3 transgenic lines were selected. Transient expression in *Nicotiana benthamiana* followed routine procedures.

Mutant genotyping and characterization

The *ubc36-2* and *ubc35-1 ubc36-2* mutants were genotyped using primers listed in Supplemental Data Set 12. Primers for the *ACTIN2* gene were used as a control. Detection of *UBC35*/*36* transcripts was performed by RT-PCR of total RNA using a Veriti Thermal cycler (Applied Biosystem). Briefly, 1 µg of RNA was subjected to reverse transcription using a High Capacity Reverse Transcription kit from Applied Biosystems. PCR was performed using primers for *UBC35* (22 cycles), *UBC36* (22 cycles), and *ACTIN2* (20 cycles). RT-PCR analyses were done in duplicate.

Protein extraction and protein gel blot analysis

Total proteins were extracted from a pool of twelve-day-old plants. Proteins were separated on a 10% Bis-Tris NuPage gel (ThermoFisher Scientific) and transferred onto a nitrocellulose membrane. For protein detection, the following antibodies were used: Monoclonal anti-GFP horseradish peroxidase-coupled (Miltenyi Biotech 130-091-833, 1/5,000), anti-UBC13 (ThermoFisher Scientific 37-1100, 1/1,500), anti-Ub (Cell Signaling P4D1 3936, 1/2,500), anti-K63 polyUb (Millipore Apu3 05-1308, 1/2,000), and anti-tubulin (Agrisera AS10 681, 1/5,000). To ascertain that no signal was carried over from one immunodetection to another, each antibody was incubated on independent membranes. Immunoblot experiments were done in duplicate.

Confocal microscopy

Plant samples were mounted in water and imaged under a Leica TCS SP8 confocal laser-scanning microscope. Images were taken of the root tips from 7-day-old Arabidopsis plants grown in the light or wild tobacco leaves. To image mCit, RFP, and HcRed, the 514-nm and 561-nm laser lines were used. Detection settings were kept constant in individual sets of experiments to allow for a comparison of the expression and localization of reporter proteins. Co-localization studies were performed using the Coloc2 plugin of ImageJ. Fluorescence intensity profiles were also obtained using ImageJ.

Whole-genome RNA profiling and bioinformatic analysis

Roots from non-induced and induced amiUBC35/36 seedlings grown for 12 days were collected, pooled, and total RNA extracted using an RNeasy kit and DNase treatment according to the supplier's instructions (Qiagen). RNA-seq experiment were carried out in triplicate. Total RNA was checked for integrity on a bioanalyzer using an RNA 6000 Pico kit (Agilent Technologies). PolyA RNA-Seq libraries were constructed from 600 ng of total RNA using a TruSeq Stranded mRNA kit (Illumina) according to the manufacturer's recommendations. Libraries were pooled in equimolar proportions and sequenced (Single Read 75pb) on an Illumina NextSeq500 instrument, using a NextSeq 500 High Output 75 Cycles kit. Demultiplexing was performed (bcl2fastq2 V2.15.0) and adapters removed (Cutadapt1.9.1). Reads were mapped onto the *Arabidopsis thaliana* genome (TAIR10 version 2017) with TopHat2. Mapped reads were assigned to features using featureCounts 1.5.0-p2, and differential analysis was performed using DESeq2. Hierarchical clustering was performed with Hierarchical Clustering Explorer (www.cs.umd.edu/hcil/hce) on normalized Log2(gene

count) using Euclidean distance. Gene ontology (GO) enrichment analysis was performed using TAIR (PANTHER GO-Slim Biological Process, GO Ontology database released 2019).

Interactome analyses

The Y2H high throughput binary interactome mapping pipeline used here was performed in liquid medium as recently reported (Monachello et al., 2019), and is an adaptation of the solid medium protocol used in the AI-1 project (Dreze et al., 2010). Briefly, low copy number yeast expression vectors expressing DB-X and AD-Y hybrid proteins and the two yeast two-hybrid strains *Saccharomyces cerevisiae* Y8930 and Y8800 were used. Yeast genome-integrated *GAL2-ADE2* and *LYS2:GAL1-HIS3* were used as reporter genes. Expression of the *GAL1-HIS3* reporter gene was tested using 1 mM 3AT (3-amino-1,2,4- triazole, a competitive inhibitor of the HIS3 gene product). Yeast strains Y8800 MATa and Y8930 MATα were transformed with AD-Y and DB-X constructs, respectively. Prior to Y2H screening, the DB-X strains were tested for their ability to auto-activate *GAL1-HIS3* reporter gene expression in the absence of AD-fusion protein. In case of autoactivation, DB-X constructs were removed from the baits and assayed in a reverse screen against the DB-AtORFeome library using their AD-X fusion.

Yeast strains expressing DB-X bait were individually grown (30°C for 72 h) in 5 mL of selective medium (Sc-Leucine; Sc-Leu) and pooled (maximum of 50 individual bait yeast strains). The 127 96-well plates of the (AD)-AtORFeome library were replicated into 32 384-well plates filled with selective medium (Sc-Tryptophan; Sc-Trp) using the colony picker Qpix2 XT and incubated at 30 °C for 72 h. DB-bait pools and the AD-library were replicated into mating plates filled with YEPD medium and incubated at 30 °C for 24 h. Mating plates were then replicated into screening plates filled with Sc-Leu-Trp-Histidine + 1 mM 3AT medium and incubated at 30 °C for 5 days. Only diploid yeast cells with interacting pairs could grow in this medium. In order to identify primary positives cultures, the Optical Density at 600 nm (OD_{600}) values of the yeast cultures were measured using a Tecan Infinite M200 PRO microplate reader. Cultures identified as harboring positive interactions were picked from selective medium and protein pairs were identified by depooling of DB-baits in a similar but targeted matricial liquid assay in which all DB-baits were individually tested against all positive AD-proteins. Identified pairs were cherry-picked and checked by PCR and DNA sequencing. Interaction networks were designed with Cytoscape.

Immunoprecipitation

Immunoprecipitation experiments were performed using 12-day-old-seedlings from wild-type, GFP, Vx3K0-NLS-mCit, and Vx3NB-NLS-mCit plants. Care was taken to use transgenic lines harboring similar amounts of transgene-expressed proteins. To extract total proteins, tissues were ground in liquid nitrogen and resuspended in ice-cold RIPA buffer (50 mM Tris-HCl pH 7.4, 150 mM NaCl, 1% Igepal, 0.5% sodium deoxycholate, 0.1% SDS) amended with protease inhibitors and 20 mM N-ethylmaleimide (NEM) to inhibit deubiquitinases during protein preparation. The samples were solubilized at 4°C for 30 minutes before centrifugation at 14,000 x g for 15 minutes at 4°C to eliminate cell debris. Supernatants were subjected to immunoprecipitation with a µMACS GFP Isolation kit (Miltenyi Biotec). To extract nuclear proteins and validate nuclear hits from the K63 ubiquitome, tissues were ground in liquid nitrogen and resuspended in ice-cold extraction buffer A (20 mM Tris-HCl pH 8.0, 0.4 M sucrose, 10 mM $MgCl_2$, 5 mM ß-mercaptoethanol, 20 mM NEM, protease inhibitors). After filtration, the extracts were centrifuged at 100 x g for 20 minutes at 4°C and the pellet resuspended in ice-cold extraction buffer B (10 mM Tris-HCl pH 8.0, 0.25 M sucrose, 10 mM $MgCl_2$, 5 mM ß-mercaptoethanol, 1% Triton X-100, 20 mM NEM, protease inhibitors). The extracts were centrifuged at 4000 x g for 10 minutes at 4°C and the pellet resuspended in ice-cold extraction buffer C (10 mM Tris-HCl pH 8.0, 1.7 M sucrose, 2 mM $MgCl_2$, 5 mM ß-mercaptoethanol, 0.15% Triton X-100, 20 mM NEM, protease inhibitors). The nuclei were pelleted at 20,000 x g before being lysed in nuclear lysis buffer (50 mM Tris-HCl pH 8.0, 0.1% SDS, 10 mM EDTA, 20 mM NEM, protease inhibitors, 10u DNAse I). After centrifugation for 10 minutes at 10,000 x g, the supernatant corresponded to the total nuclear fraction. Total nuclear fractions were subjected to immunoprecipitation with a µMACS GFP Isolation kit (Miltenyi Biotec). Immunoprecipitates were eluted off of the beads using Laemmli buffer. The samples were boiled for 2 minutes at 95°C and separated on a 10% Bis-Tris NuPage Gel (ThermoFisher Scientific).

Mass spectrometry and data analyses

Immunoprecipitates were separated for 10 minutes on a 10% Bis-Tris NuPage Gel (Life Technologies) and subjected to Coomassie blue staining before the bands were cut off. In-gel trypsin digestion, reduction, and alkylation followed previously published procedures (Shevchenko et al., 2006; Szabo et al., 2018). Peptides were analyzed separately by nanoLC-MS/MS in a Triple-TOF 4600 mass spectrometer (AB Sciex) coupled to a nanoRSLC ultra performance liquid chromatography (UPLC) system (Thermo Scientific) equipped with a trap

column (Acclaim PepMap100C18, 75 µmi.d.× 2 cm, 3 µm) and an analytical column (Acclaim PepMapRSLCC18, 75 µmi.d.× 50 cm, 2 µm, 100 Å). Peptides were loaded at 5 µl/min with 0.05% TFA in 5% acetonitrile and separated at a flow rate of 300 nl/min with a 5 to 35% solvent B gradient for 120 min. Solvent A was 0.1% formic acid in water, and solvent B was 0.1% formic acid in 100% acetonitrile. NanoLC-MS/MS experiments were conducted using the Data Dependent Acquisition method by selecting the 20 most intense precursors for CID fragmentation with Q1 quadrupole set at low resolution for better sensitivity. The identification of K63 ubiquitome by mass spectrometry was done in duplicate.

Raw data were processed with MS Data Converter software (AB Sciex) to generate .mgf data files, and protein identification were performed using the MASCOT search engine (Matrix Science, London, UK) against the TAIR10 database (version 2017) with carbamidomethylation of cysteines set as the fixed modification and oxidation of methionines and ubiquitinylation (Gly-Gly) of lysine as the variable modifications. Peptide and fragment tolerance were respectively set at 20 ppm and 0.05 Da. Results were analyzed with Scaffold 4.0 software (Proteome Software). Proteins were considered to be part of the K63 ubiquitome when identified using at least two unique peptides at a 95% probability level for both peptides and proteins. GO enrichment analysis of the target proteins from the K63 ubiquitome was performed using TAIR (PANTHER GO-Slim Biological Process, GO Ontology database released 2019). The subcellular localizations of proteins were predicted using SUBA3 (Tanz et al., 2013).

Accession Numbers

Sequence data from this article can be found in the GenBank/EMBL libraries under the following accession numbers: *UBC35* (At1g78870), *UBC36* (At1g16890), *H2AX* (At1g08880), *H2B.11* (At5g59910), *MEE5* (At1g06220), *SUN1* (At5g04990), *SUN2* (At3g10730), *ACTIN2* (At3g18780). The identifiers of the T-DNA mutants used in this study are *ubc35-1* (WiscDsLox323H12), *ubc36-1* (SALK_047381), and *ubc36*-2 (GABI_836B11). RNA-seq data were deposited at Array Express (accession number E-MTAB-8437; www.ebi.ac.uk/arrayexpress).

Supplemental Data

Supplemental Figure 1. Characterization of Arabidopsis loss-of-function mutants for *UBC35* and *UBC36*.

Supplemental Figure 2. K63 polyubiquitin networks revealed by interactome analysis.

Supplemental Figure 3. Subcellular localization of UBC35 and UBC36.

Supplemental Figure 4. Co-localization analysis of Vx3K0-NLS-mCit with SR34-RFP and HcRed-SERRATE.

Supplemental Figure 5. Immunoprecipitation of the Vx3K0-NLS-mCit and Vx3NB-NLS-mCit sensors.

Supplemental Figure 6. Coomassie blue staining of Vx3K0-NLS-mCit and Vx3NB-NLS-mCit immunoprecipitates.

Supplemental Table 1. Representation of E3 ligases in the Arabidopsis genome, as reported by Mazzucotelli et al. (2006), and in the 12,000 ORF library.

Supplemental Data Set 1. List of genes upregulated in estradiol-induced amiUBC35/36 lines compared to non-induced (padj<0.01, Fold change >1.5).

Supplemental Data Set 2. List of genes downregulated in estradiol-induced amiUBC35/36 lines compared to non-induced (padj<0.01, Fold change >1.5).

Supplemental Data Set 3. Gene ontology (GO) enrichment analysis on upregulated genes in estradiol-induced amiUBC35/36 lines.

Supplemental Data Set 4. Gene ontology (GO) enrichment analysis on downregulated genes in estradiol-induced amiUBC35/36 lines.

Supplemental Data Set 5. List of primary interacting proteins identified with UBC35/36 and UEV1A-D used as baits against the 12,000 ORF library.

Supplemental Data Set 6. List of interacting proteins identified by ORF-based yeast two hybrid interactome within this study (12k_space, InterATOME; 8k_space, AI1; LCI, literature-curated interaction).

Supplemental Data Set 7. List of interacting proteins identified with UBC35/36 and UEV1A-D combing the 12,000 ORF library, the published Arabidopsis 8,000 ORF-based interactome and literature-curated interactions.

Supplemental Data Set 8. List of proteins identified by sensor-based proteomics using the Vx3K0-NLS-mCit sensor line.

Supplemental Data Set 9. Gene ontology (GO) enrichment analysis on proteins identified by sensor-based proteomics.

Supplemental Data Set 10. List of nuclear proteins identified by sensor-based proteomics using the Vx3K0-NLS-mCit sensor line.

Supplemental Data Set 11. Gene ontology (GO) enrichment analysis on nuclear proteins identified by sensor-based proteomics.

Supplemental Data Set 12. List of primers used in this study.

ACKNOWLEDGMENTS

This work has benefited from the expertise of the high throughput sequencing and imaging core facilities of I2BC and LRSV. We are thankful to David Cornu from the I2BC SICaPS proteomic facility for mass spectrometry analysis. We also thank Robert Cohen (Colorado State University, Fort Collins, CO, USA) and Katja Graumann (Oxford Brookes University, Oxford, England) for sharing the K63 sensor constructs and SUN1:SUN1-GFP or SUN2:SUN2-GFP binary vectors, respectively. This work was supported by grants from Marie Curie Action (to G.V, PCIG-GA-2012-334021), Agence Nationale de la Recherche (to G.V; ANR-13-JSV2-0004-01), the French Laboratory of Excellence project "TULIP" (to G.V.; ANR-10-LABX-41; ANR-11-IDEX-0002-02), and "Saclay Plant Sciences-SPS" (to G.V, D.M., and C.L.; ANR-10-LABX-0040-SPS) to G.V., D.M, and C.L.

AUTHOR CONTRIBUTIONS

N.R.-B. characterized the sensor lines and performed the proteomic analysis, D.M. performed the interactome analysis, U.D. carried out the colocalization experiments with nuclear body markers, A.W. generated amiUBC35/36 lines and performed the RNA-seq experiments,

H.S.C. analyzed the RNA-seq data, A.C. isolated and characterized the *ubc35* and *ubc36* mutants, A.J. studied the subcellular localization of UBC35 and UBC36, C.L. supervised and analyzed the interactome data, and G.V. conceived the project, designed the experiments, analyzed the data, and wrote the article.

Table 1. Examples of proteins and biological processes involving nuclear proteins targeted by K63 polyubiquitination identified in the current study.

RNA		
AT1G06220	MEE5	Homolog of splicing factor Snu114
AT1G20960	BRR2	DEAD/DExH box ATP-dependent RNA helicase
AT1G72730		DEA(D/H)-box RNA helicase family
AT1G80070	PRP8	pre-mRNA splicing
AT3G58510		DEA(D/H)-box RNA helicase
AT5G07350	TSN1	RNA binding protein with nuclease activity
AT5G26742	ATRH3	DEAD box RNA helicase
Nuclear transport		
AT1G14850	NUP155	Nucleoporin
AT1G68910	WIT2	Nuclear envelope docking of RANGAP
AT1G79280	NUA	Nuclear pore anchor
AT2G05120	NUP133	Nucleoporin
AT3G10650		Nucleoporin involved in mRNA export
AT3G63130	RANGAP1	GTPase activating protein involved in nuclear export
AT4G16143	IMPA-2	Importin alpha isoform 2
AT5G20200		Nucleoporin-like protein
Chromatin		
AT1G07660	H4	Histone H4
AT1G52740	H2A.9	Histone H2A
AT2G28720	H2B.3	Histone H2B
AT1G08880	H2AX	Histone H2AX
AT3G06400	CHR11	Chromatin remodeling factor
AT3G45980	H2B.9	Histone H2B
AT5G59910	H2B.11	Histone H2B
Nucleus structure		
AT1G67230	LINC1	Peripheral nuclear coiled-coil protein
AT3G10730	SUN2	Cytoskeletal-nucleoskeletal bridging complex
AT5G04990	SUN1	Cytoskeletal-nucleoskeletal bridging complex
AT5G65770	LINC4	Peripheral nuclear coiled-coil protein

References

Adhikari, A., and Chen, Z.J. (2009). Diversity of polyubiquitin chains. Dev Cell **16,** 485-486.

Adhikary, S., Marinoni, F., Hock, A., Hulleman, E., Popov, N., Beier, R., Bernard, S., Quarto, M., Capra, M., Goettig, S., Kogel, U., Scheffner, M., Helin, K., and Eilers, M. (2005). The ubiquitin ligase HectH9 regulates transcriptional activation by Myc and is essential for tumor cell proliferation. Cell **123,** 409-421.

Andersen, P.L., Zhou, H., Pastushok, L., Moraes, T., McKenna, S., Ziola, B., Ellison, M.J., Dixit, V.M., and Xiao, W. (2005). Distinct regulation of Ubc13 functions by the two ubiquitin-conjugating enzyme variants Mms2 and Uev1A. J Cell Biol **170,** 745-755.

Arabidopsis Interactome Mapping, C. (2011). Evidence for network evolution in an Arabidopsis interactome map. Science **333,** 601-607.

Back, S., Gorman, A.W., Vogel, C., and Silva, G.M. (2019). Site-Specific K63 Ubiquitinomics Provides Insights into Translation Regulation under Stress. Journal of proteome research **18,** 309-318.

Barberon, M., Zelazny, E., Robert, S., Conejero, G., Curie, C., Friml, J., and Vert, G. (2011). Monoubiquitin-dependent endocytosis of the iron-regulated transporter 1 (IRT1) transporter controls iron uptake in plants. Proc Natl Acad Sci U S A **108,** E450-458.

Bertrand, M.J., Milutinovic, S., Dickson, K.M., Ho, W.C., Boudreault, A., Durkin, J., Gillard, J.W., Jaquith, J.B., Morris, S.J., and Barker, P.A. (2008). cIAP1 and cIAP2 facilitate cancer cell survival by functioning as E3 ligases that promote RIP1 ubiquitination. Mol Cell **30,** 689-700.

Clough, S.J., and Bent, A.F. (1998). Floral dip: A simplified method for Agrobacterium-mediated transformation of *Arabidopsis thaliana*. Plant J. **16,** 735-743.

Dreze, M., Monachello, D., Lurin, C., Cusick, M.E., Hill, D.E., Vidal, M., and Braun, P. (2010). High-quality binary interactome mapping. Methods Enzymol **470,** 281-315.

Dubeaux, G., Neveu, J., Zelazny, E., and Vert, G. (2018). Metal Sensing by the IRT1 Transporter-Receptor Orchestrates Its Own Degradation and Plant Metal Nutrition. Mol Cell **69,** 953-964 e955.

Gavin, A.C., Bosche, M., Krause, R., Grandi, P., Marzioch, M., Bauer, A., Schultz, J., Rick, J.M., Michon, A.M., Cruciat, C.M., Remor, M., Hofert, C., Schelder, M., Brajenovic, M., Ruffner, H., Merino, A., Klein, K., Hudak, M., Dickson, D., Rudi, T., Gnau, V., Bauch, A., Bastuck, S., Huhse, B., Leutwein, C., Heurtier, M.A., Copley, R.R., Edelmann, A., Querfurth, E., Rybin, V., Drewes, G., Raida, M., Bouwmeester, T., Bork, P., Seraphin, B., Kuster, B., Neubauer, G., and Superti-Furga, G. (2002). Functional organization of the yeast proteome by systematic analysis of protein complexes. Nature **415,** 141-147.

Gremski, K., Ditta, G., and Yanofsky, M.F. (2007). The HECATE genes regulate female reproductive tract development in Arabidopsis thaliana. Development **134,** 3593-3601.

Guo, H., Wen, R., Wang, Q., Datla, R., and Xiao, W. (2016). Three Brachypodium distachyon Uev1s Promote Ubc13-Mediated Lys63-Linked Polyubiquitination and Confer Different Functions. Front Plant Sci **7,** 1551.

Hjerpe, R., Aillet, F., Lopitz-Otsoa, F., Lang, V., England, P., and Rodriguez, M.S. (2009). Efficient protection and isolation of ubiquitylated proteins using tandem ubiquitin-binding entities. EMBO Rep **10,** 1250-1258.

Hodge, C.D., Spyracopoulos, L., and Glover, J.N. (2016). Ubc13: the Lys63 ubiquitin chain building machine. Oncotarget **7,** 64471-64504.

Hofmann, R.M., and Pickart, C.M. (1999). Noncanonical MMS2-encoded ubiquitin-conjugating enzyme functions in assembly of novel polyubiquitin chains for DNA repair. Cell **96,** 645-653.

Hofmann, R.M., and Pickart, C.M. (2001). In vitro assembly and recognition of Lys-63 polyubiquitin chains. J Biol Chem **276,** 27936-27943.

Johnson, A., and Vert, G. (2016). Unraveling K63 Polyubiquitination Networks by Sensor-Based Proteomics. Plant Physiol **171,** 1808-1820.

Kim, D.Y., Scalf, M., Smith, L.M., and Vierstra, R.D. (2013). Advanced proteomic analyses yield a deep catalog of ubiquitylation targets in Arabidopsis. Plant Cell **25,** 1523-1540.

Kim, H.C., and Huibregtse, J.M. (2009). Polyubiquitination by HECT E3s and the determinants of chain type specificity. Mol Cell Biol **29,** 3307-3318.

Kim, W., Bennett, E.J., Huttlin, E.L., Guo, A., Li, J., Possemato, A., Sowa, M.E., Rad, R., Rush, J., Comb, M.J., Harper, J.W., and Gygi, S.P. (2011). Systematic and quantitative assessment of the ubiquitin-modified proteome. Mol Cell **44,** 325-340.

Kirisako, T., Kamei, K., Murata, S., Kato, M., Fukumoto, H., Kanie, M., Sano, S., Tokunaga, F., Tanaka, K., and Iwai, K. (2006). A ubiquitin ligase complex assembles linear polyubiquitin chains. EMBO J **25,** 4877-4887.

Komander, D., and Rape, M. (2012). The Ubiquitin Code. Annual Review of Biochemistry, Vol 81 **81,** 203-229.

Kraft, E., Stone, S.L., Ma, L., Su, N., Gao, Y., Lau, O.S., Deng, X.W., and Callis, J. (2005). Genome analysis and functional characterization of the E2 and RING-type E3 ligase ubiquitination enzymes of Arabidopsis. Plant Physiol **139,** 1597-1611.

Li, W., and Schmidt, W. (2010). A lysine-63-linked ubiquitin chain-forming conjugase, UBC13, promotes the developmental responses to iron deficiency in Arabidopsis roots. Plant J **62,** 330-343.

Lim, K.L., and Lim, G.G. (2011). K63-linked ubiquitination and neurodegeneration. Neurobiol Dis **43,** 9-16.

Lorkovic, Z.J., Hilscher, J., and Barta, A. (2008). Co-localisation studies of Arabidopsis SR splicing factors reveal different types of speckles in plant cell nuclei. Exp Cell Res **314,** 3175-3186.

Mattiroli, F., Vissers, J.H., van Dijk, W.J., Ikpa, P., Citterio, E., Vermeulen, W., Marteijn, J.A., and Sixma, T.K. (2012). RNF168 ubiquitinates K13-15 on H2A/H2AX to drive DNA damage signaling. Cell **150,** 1182-1195.

Mazzucotelli, E., Belloni, S., Marone, D., De Leonardis, A., Guerra, D., Di Fonzo, N., Cattivelli, L., Mastrangelo, A. (2006). The e3 ubiquitin ligase gene family in plants: regulation by degradation. Curr Genomics **7,** 509-522.

Monachello, D., Guillaumot, D., and Lurin, C. (2019). A pipeline for systematic yeast 2-hybrid matricial screening in liquid culture. Protocol Exchange.

Mukhopadhyay, D., and Riezman, H. (2007). Proteasome-independent functions of ubiquitin in endocytosis and signaling. Science **315,** 201-205.

Mukhtar, M.S., Carvunis, A.R., Dreze, M., Epple, P., Steinbrenner, J., Moore, J., Tasan, M., Galli, M., Hao, T., Nishimura, M.T., Pevzner, S.J., Donovan, S.E., Ghamsari, L., Santhanam, B., Romero, V., Poulin, M.M., Gebreab, F., Gutierrez, B.J., Tam, S., Monachello, D., Boxem, M., Harbort, C.J., McDonald, N., Gai, L., Chen, H., He, Y., European Union Effectoromics C., Vandenhaute, J., Roth, F.P., Hill, D.E., Ecker, J.R., Vidal, M., Beynon, J., Braun, P., Dangl, J.L. (2011). Independently evolved virulence effectors converge onto hubs in a plant immune system network. Science **333,** 596-601.

Mural, R.V., Liu, Y., Rosebrock, T.R., Brady, J.J., Hamera, S., Connor, R.A., Martin, G.B., and Zeng, L. (2013). The tomato Fni3 lysine-63-specific ubiquitin-conjugating enzyme and suv ubiquitin E2 variant positively regulate plant immunity. Plant Cell **25,** 3615-3631.

Nakada, S., Tai, I., Panier, S., Al-Hakim, A., Iemura, S., Juang, Y.C., O'Donnell, L., Kumakubo, A., Munro, M., Sicheri, F., Gingras, A.C., Natsume, T., Suda, T., and Durocher, D. (2010). Non-canonical inhibition of DNA damage-dependent ubiquitination by OTUB1. Nature **466,** 941-946.

Pan, I.C., and Schmidt, W. (2014). Functional implications of K63-linked ubiquitination in the iron deficiency response of Arabidopsis roots. Front Plant Sci **4,** 542.

Peng, J., Schwartz, D., Elias, J.E., Thoreen, C.C., Cheng, D., Marsischky, G., Roelofs, J., Finley, D., and Gygi, S.P. (2003). A proteomics approach to understanding protein ubiquitination. Nat Biotechnol **21,** 921-926.

Pickart, C.M., and Fushman, D. (2004). Polyubiquitin chains: polymeric protein signals. Curr Opin Chem Biol **8,** 610-616.

Raczynska, K.D., Stepien, A., Kierzkowski, D., Kalak, M., Bajczyk, M., McNicol, J., Simpson, C.G., Szweykowska-Kulinska, Z., Brown, J.W., and Jarmolowski, A. (2014). The SERRATE protein is involved in alternative splicing in Arabidopsis thaliana. Nucleic Acids Res **42,** 1224-1244.

Romero-Barrios, N., and Vert, G. (2018). Proteasome-independent functions of lysine-63 polyubiquitination in plants. New Phytol **217,** 995-1011.

Schuster, C., Gaillochet, C., and Lohmann, J.U. (2015). Arabidopsis HECATE genes function in phytohormone control during gynoecium development. Development **142,** 3343-3350.

Sheng, Y., Hong, J.H., Doherty, R., Srikumar, T., Shloush, J., Avvakumov, G.V., Walker, J.R., Xue, S., Neculai, D., Wan, J.W., Kim, S.K., Arrowsmith, C.H., Raught, B., and Dhe-Paganon, S. (2012). A human ubiquitin conjugating enzyme (E2)-HECT E3 ligase structure-function screen. Mol Cell Proteomics **11,** 329-341.

Shevchenko, A., Tomas, H., Havlis, J., Olsen, J.V., and Mann, M. (2006). In-gel digestion for mass spectrometric characterization of proteins and proteomes. Nat Protoc **1,** 2856-2860.

Silva, G.M., Finley, D., and Vogel, C. (2015). K63 polyubiquitination is a new modulator of the oxidative stress response. Nat Struct Mol Biol **22,** 116-123.

Sims, J.J., Scavone, F., Cooper, E.M., Kane, L.A., Youle, R.J., Boeke, J.D., and Cohen, R.E. (2012). Polyubiquitin-sensor proteins reveal localization and linkage-type dependence of cellular ubiquitin signaling. Nat Methods **9,** 303-309.

Szabo, A., Papin, C., Cornu, D., Chelot, E., Lipinszki, Z., Udvardy, A., Redeker, V., Mayor, U., and Rouyer, F. (2018). Ubiquitylation Dynamics of the Clock Cell Proteome and TIMELESS during a Circadian Cycle. Cell Rep **23,** 2273-2282.

Tanz, S.K., Castleden, I., Hooper, C.M., Vacher, M., Small, I., and Millar, H.A. (2013). SUBA3: a database for integrating experimentation and prediction to define the SUBcellular location of proteins in Arabidopsis. Nucleic Acids Res **41,** D1185-1191.

Turek, I., Tischer, N., Lassig, R., and Trujillo, M. (2018). Multi-tiered pairing selectivity between E2 ubiquitin-conjugating enzymes and E3 ligases. J Biol Chem **293,** 16324-16336.

Udeshi, N.D., Svinkina, T., Mertins, P., Kuhn, E., Mani, D.R., Qiao, J.W., and Carr, S.A. (2013). Refined preparation and use of anti-diglycine remnant (K-epsilon-GG) antibody enables routine quantification of 10,000s of ubiquitination sites in single proteomics experiments. Mol Cell Proteomics **12,** 825-831.

van Wijk, S.J., Fiskin, E., Putyrski, M., Pampaloni, F., Hou, J., Wild, P., Kensche, T., Grecco, H.E., Bastiaens, P., and Dikic, I. (2012). Fluorescence-Based Sensors to Monitor Localization and Functions of Linear and K63-Linked Ubiquitin Chains in Cells. Mol Cell.

Walton, A., Stes, E., Cybulsi, N., Van Bel, M., Inigo, S., Nagels Durand, A., Timmerman, E., Heyman, J., Pauwels, L., De Veylder, L., Goosens, A., De Smet, Y., Coppens, F., Goomachtig, S., and Gevaert, K. (2016a). It's time for some "site" seeing: novel tools to monitor the ubiquitin landscape in *Arabidopsis thaliana*. Plant Cell**,** doi:10.1105/tpc.1115.00878.

Walton, A., Stes, E., Cybulski, N., Van Bel, M., Inigo, S., Durand, A.N., Timmerman, E., Heyman, J., Pauwels, L., De Veylder, L., Goossens, A., De Smet, I., Coppens, F., Goormachtig, S., and Gevaert, K. (2016b). It's Time for Some "Site"-Seeing: Novel Tools to Monitor the Ubiquitin Landscape in Arabidopsis thaliana. Plant Cell **28,** 6-16.

Wang, G., Gao, Y., Li, L., Jin, G., Cai, Z., Chao, J.I., and Lin, H.K. (2012). K63-linked ubiquitination in kinase activation and cancer. Front Oncol **2,** 5.

Wang, L., Wen, R., Wang, J., Xiang, D., Wang, Q., Zang, Y., Wang, Z., Huang, S., Li, X., Datla, R., Fobert, P.R., Wang, H., Wei, Y., and Xiao, W. (2019). Arabidopsis UBC13 differentially regulates two programmed cell death pathways in responses to pathogen and low-temperature stress. New Phytol **221,** 919-934.

Wen, R., Torres-Acosta, J.A., Pastushok, L., Lai, X., Pelzer, L., Wang, H., and Xiao, W. (2008). Arabidopsis UEV1D promotes Lysine-63-linked polyubiquitination and is involved in DNA damage response. Plant Cell **20,** 213-227.

Wen, R., Wang, S., Xiang, D., Venglat, P., Shi, X., Zang, Y., Datla, R., Xiao, W., and Wang, H. (2014). UBC13, an E2 enzyme for Lys63-linked ubiquitination, functions in root development by affecting auxin signaling and Aux/IAA protein stability. Plant J **80,** 424-436.

Woelk, T., Sigismund, S., Penengo, L., and Polo, S. (2007). The ubiquitination code: a signalling problem. Cell Div **2,** 11.

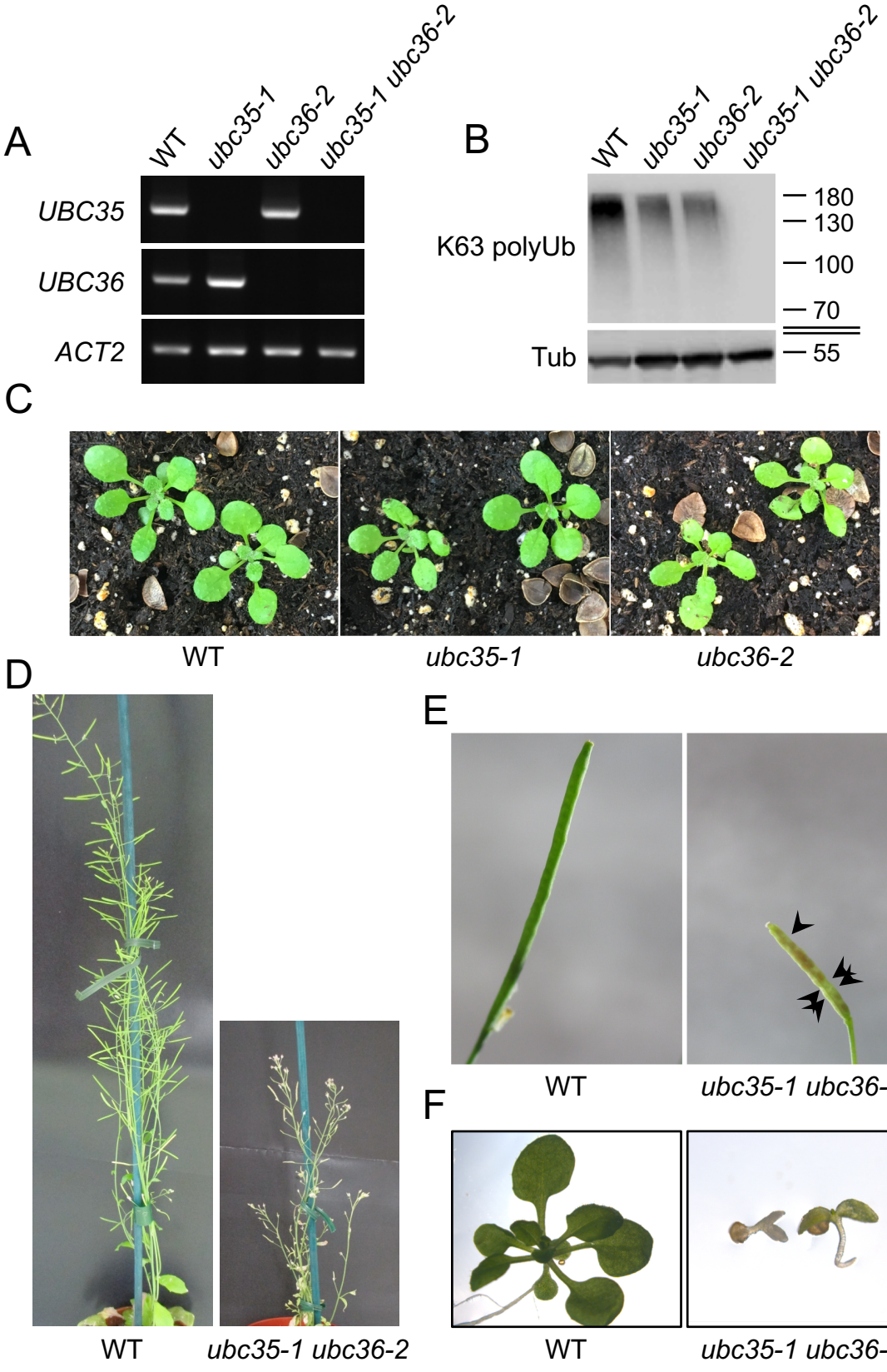

Figure 1. Characterization of Arabidopsis loss-of-function mutants for *UBC35* and *UBC36*. A, RT-PCR analysis monitoring the accumulation of *UBC35* and *UBC36* transcripts in wild type, *ubc35-1, ubc36-2* and *ubc35-1 ubc36-2* plants. Amplification of *ACTIN2* (*ACT2*) was used as a loading control. B, Accumulation of K63 polyubiquitinated proteins in total extracts from wild-type, *ubc35-1, ubc36-2* and *ubc35-1 ubc36-2* visualized by immunoblot analysis using Apu3 K63 polyUb-specific antibodies. Detection of tubulin served as a loading control. The sizes of marker proteins in kDa are shown. C, Phenotypes of 3-week-old wild-type, *ubc35-1* and *ubc36-2* plants grown in soil. D, Phenotypes of 5-week-old wild-type and *ubc35-1 ubc36-2* F2 plants grown in soil. E, Fertility defects of *ubc35-1 ubc36-2.* Arrows point to aborted seeds in siliques. F, Phenotypes of 15-day-old wild-type and *ubc35-1 ubc36-2* F3 seedlings grown *in vitro.*

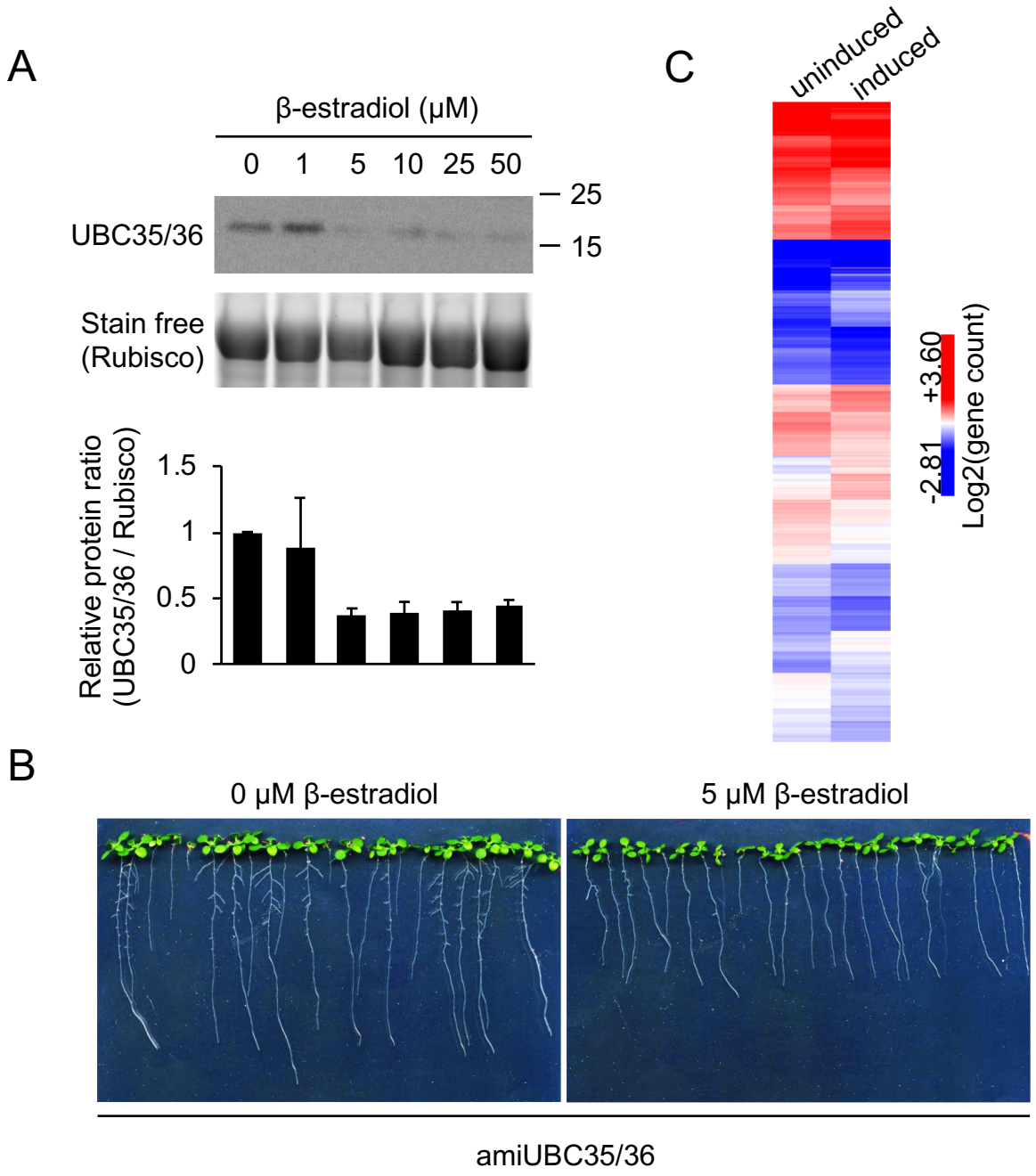

Figure 2. Characterization of inducible amiUBC35/36 lines. A, Influence of amiUBC35/36 expression on UBC35/36 protein accumulation. Total proteins were extracted from 12-day-old seedlings grown on mock or β-estradiol medium. Ub-unloaded UBC35/36 protein accumulation was monitored using anti-UBC13 antibodies. Stain free visualization of total proteins was used as a loading control. The sizes of marker proteins in kDa are shown. Quantification shows UBC35/36 protein accumulation relative to loading control, normalized to the mock-treated condition. Results are presented as mean of two independent experiments. Error bars represent standard deviation. B, Phenotypes of amiUBC35/36 lines grown for 12 days on mock (left) or plates containing 5 μM β-estradiol. C, Heatmap of differentially regulated genes upon downregulation of *UBC35/36* expression. Differentially expressed genes were clustered using Euclidean distance. Related to Figure 1.

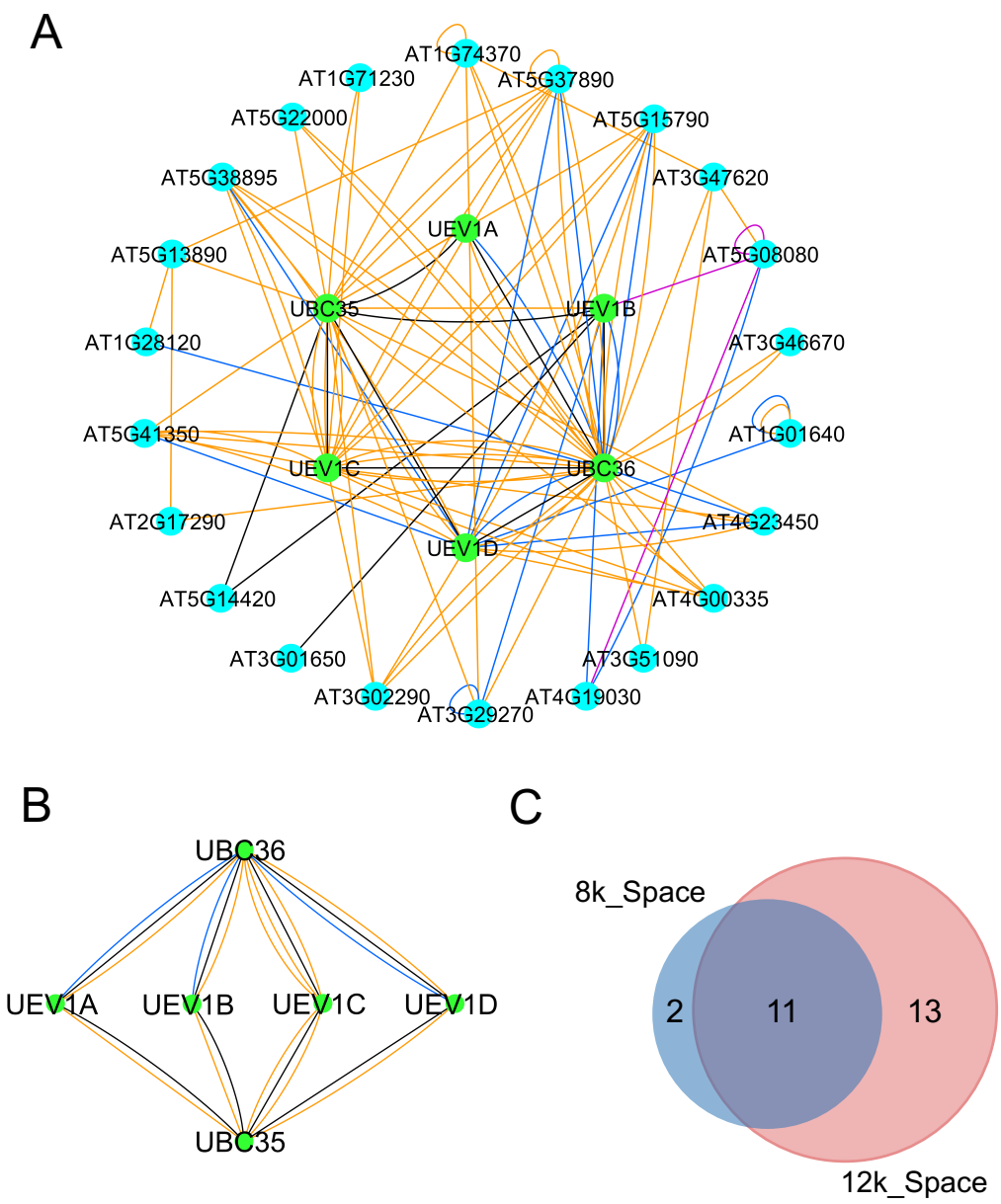

Figure 3. Identification of UBC35/36-UEV1A-D primary interacting proteins by interactome analysis. A, Primary interacting proteins of UBC35/36/UEV1A-D identified by yeast two-hybrid interactome analysis using the 12k_space ORFs from Arabidopsis. Interactions between UBC35/36/UEV1A-D-interacting proteins are also shown. B, Respective interactions between E2 and E2 variants driving K63 polyubiquitination. C, Venn diagram showing the overlap between UBC35/36-UEV1A-D primary interacting proteins coming from the 8k_Space (Arabidopsis Interactome Mapping, 2011) and the 12k_Space. Edge color: blue, Arabidopsis Interactome Map (Arabidopsis Interactome Mapping, 2011); purple, Plant Immune System Network (Mukhtar et al., 2011); black, literature-curated interactions; orange, this study.

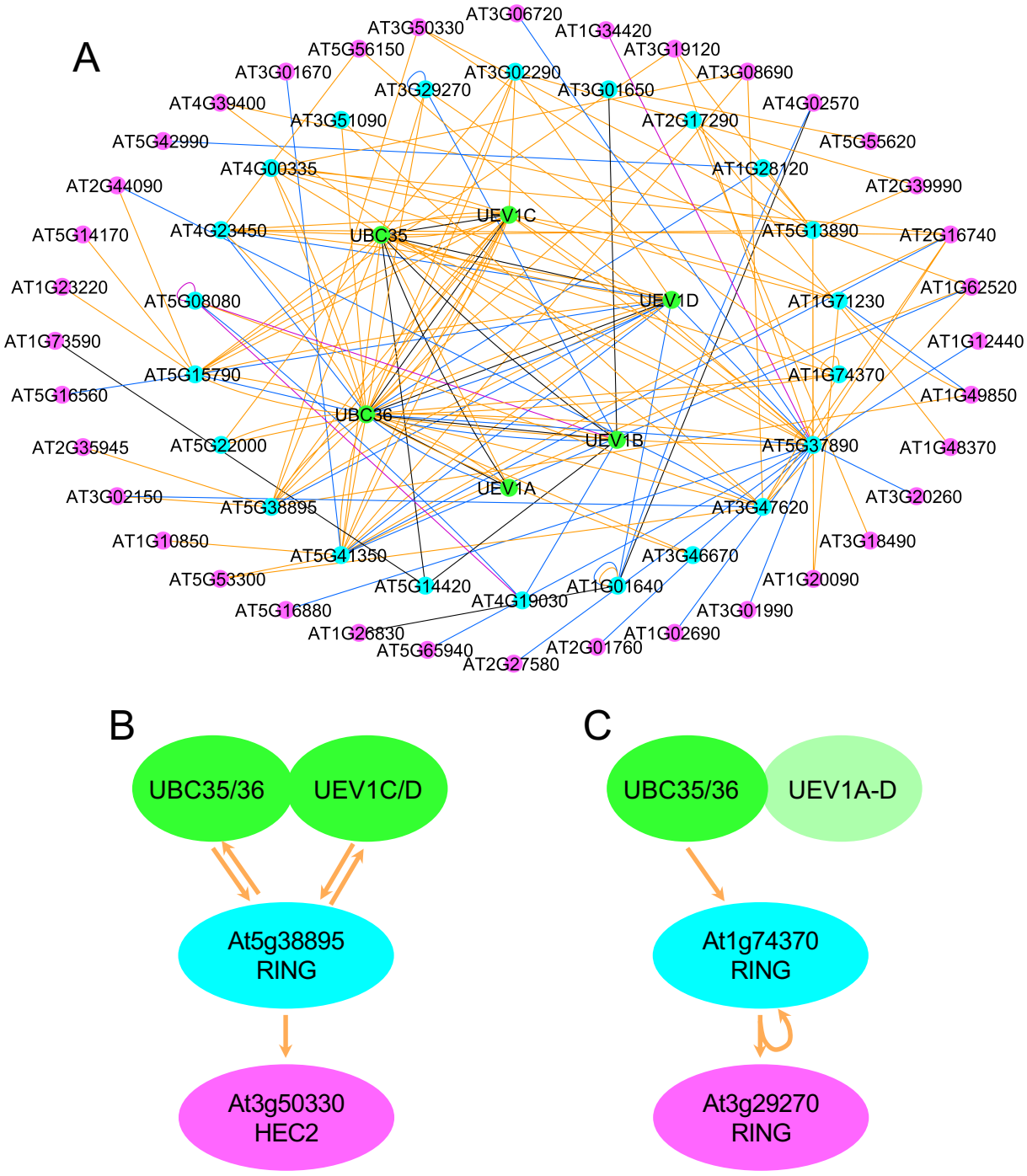

Figure 4. Identification of UBC35/36-UEV1A-D secondary interacting proteins by interactome analysis. A, Proteins interacting with primary interactants of UBC35/36/UEV1A-D from Figure 2 are shown in pink. B, C Examples of E2-E3-target reconstitution. Edge color: blue, Arabidopsis Interactome Map (Arabidopsis Interactome Mapping, 2011); purple, Plant Immune System Network (Mukhtar et al., 2011); black, literature-curated interactions; orange, this study.

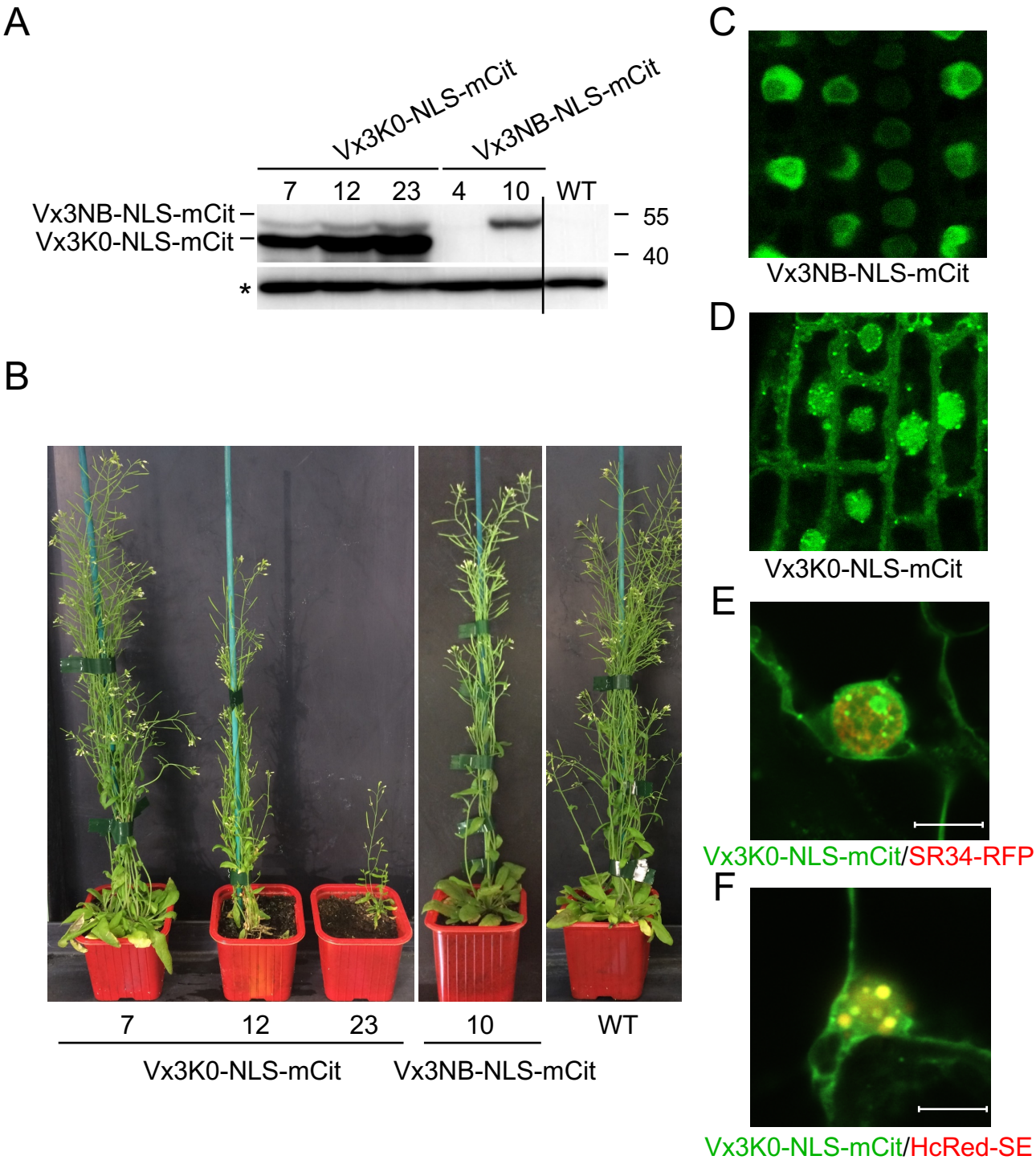

Figure 5. Characterization of Vx3K0-NLS and Vx3NB-NLS K63 polyUb sensor lines. A, Immunoblot analysis monitoring the accumulation of the Vx3K0-NLS-mCit and Vx3NB-NLS-mCit proteins in different mono-insertional homozygous transgenic lines using anti-GFP antibodies. Wild-type plants served as a negative control. The asterisk indicates a non-specific band used as a loading control. The sizes of marker proteins in kDa are shown. B, Phenotypes of 5-week-old soil-grown wild-type (WT), Vx3K0-NLS-mCit and Vx3NB-NLS-mCit transgenic lines. Lines Vx3K0-NLS-mCit 7 and Vx3NB-NLS-mCit 10 were selected for further analysis. C, D, Subcellular localization of Vx3K0-NLS-mCit (C) and Vx3NB-NLS-mCit (D) sensors in the primary roots of Arabidopsis stable transgenic lines. Scale bars = 10 µm. E, F, Colocalization analysis between Vx3K0-NLS-mCit and SR34-RFP (E) or HcRed-SERRATE (F) using transient expression in *Nicotiana benthamiana* leaves. Representative images are shown (n=10). The overlay between the green (mCit) and red (RFP or Hc-Red) channels is shown. Colocalization is revealed by the yellow color observed for Vx3K0-NLS-mCit and HcRed-SE nuclear bodies. Scale bars = 10 µM.

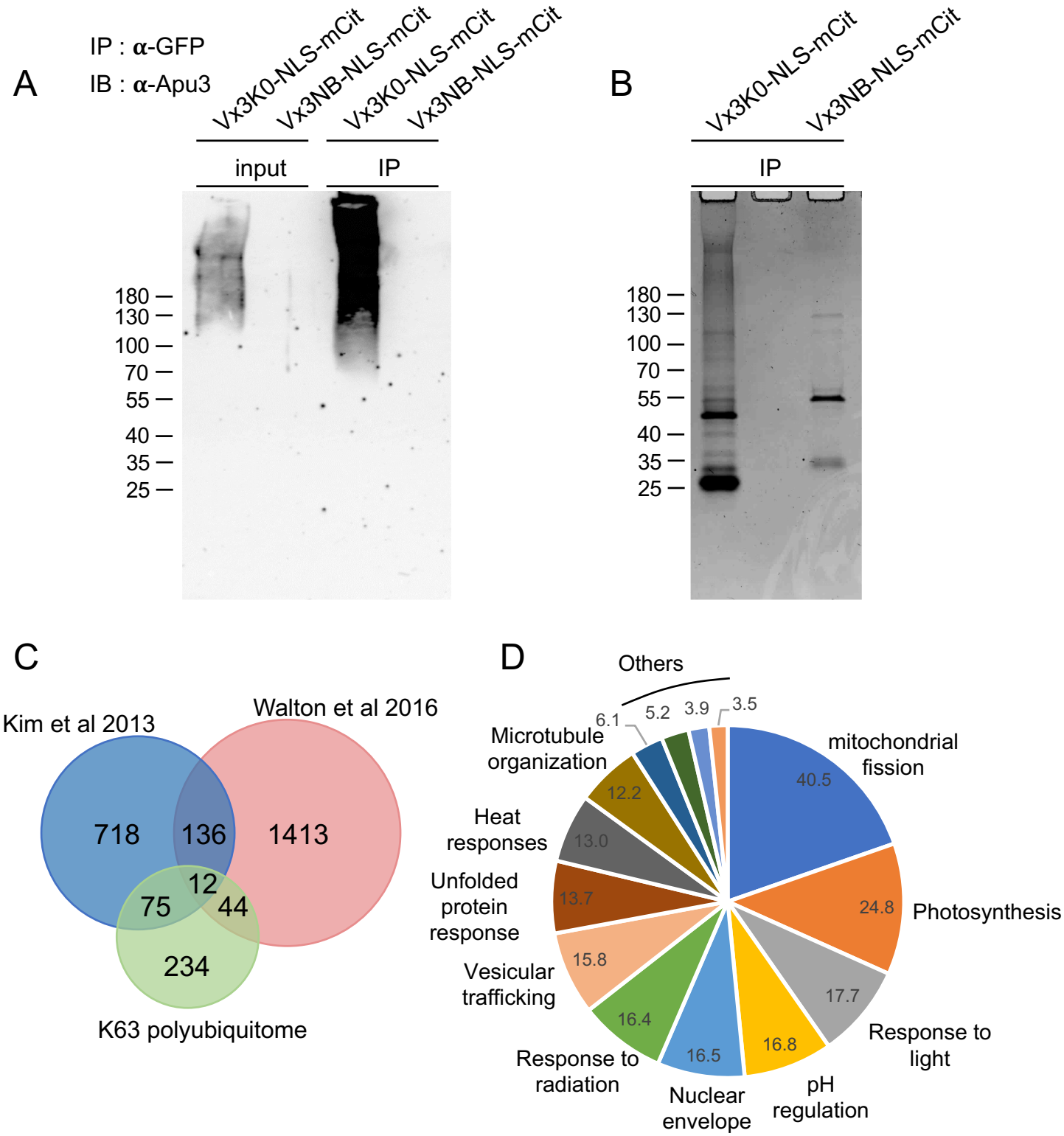

Figure 6. Isolation and analysis of the Arabidopsis K63 ubiquitome. A, Sensor-based immunoprecipitation of proteins carrying K63 polyUb chains. Immunoprecipitation was performed using anti-GFP antibodies on RIPA buffer-solubilized protein extracts from mono-insertional homozygous plants expressing Vx3K0-NLS-mCit and the negative control Vx3NB-NLS-mCit. Extracts were subjected to immunoblotting with anti-GFP antibodies (see Supplemental Figure 6) to assess immunoprecipitation efficiency, and with anti-K63 polyUb Apu3 antibodies. IB, immunoblotting; IP, immunoprecipitation. The sizes of marker proteins in kDa are shown. B, Coomassie blue staining of Vx3K0-NLS-mCit and Vx3NB-NLS-mCit immunoprecipitates shown in (A). C, Venn diagram showing the overlap between proteins carrying K63 polyUb chains purified by sensor-based proteomics and the non-linkage-resolutive TUBE/USU and COFRADIC ubiquitomes (Kim et al., 2013; Walton et al., 2016). D, GO term enrichment of K63 polyubiquitinated proteins identified by mass spectrometry. The enrichment fold is shown.

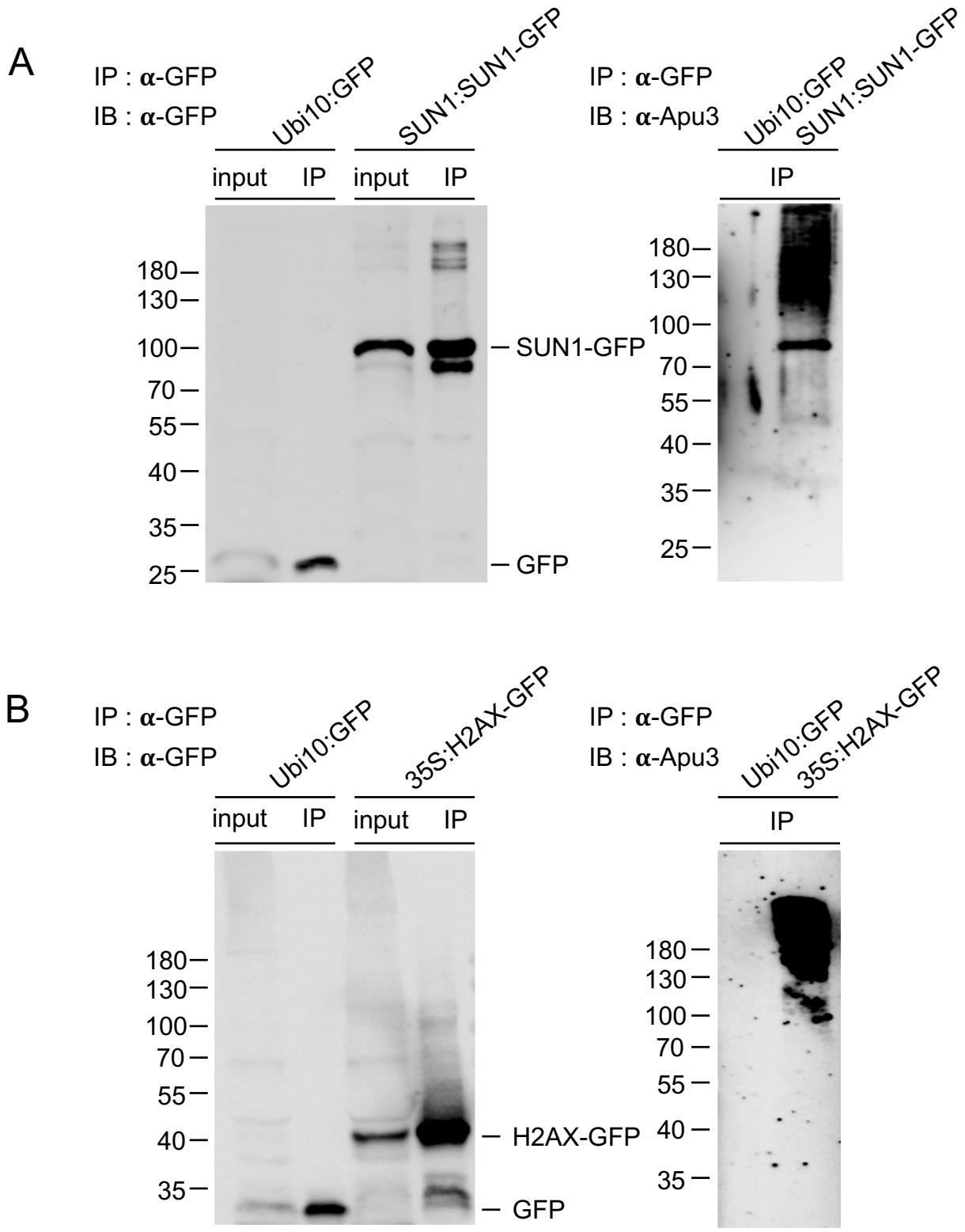

Figure 7. Validation of *in planta* K63 polyubiquitination for nuclear hits identified by sensor-based proteomics. A, B, *In vivo* K63 polyubiquitination of SUN1 and H2AX. Immunoprecipitation was performed using anti-GFP antibodies on RIPA buffer-solubilized protein extracts from mono-insertional homozygous SUN1:SUN1-GFP (A) and 35S:H2AX-GFP (B) transgenic lines. Plants expressing free GFP were used as a negative control. Input and IP samples were subjected to immunoblotting with anti-GFP and anti-K63 polyUb antibodies (Apu3). IB, immunoblotting, IP, immunoprecipitation. The sizes of marker proteins in kDa are shown.

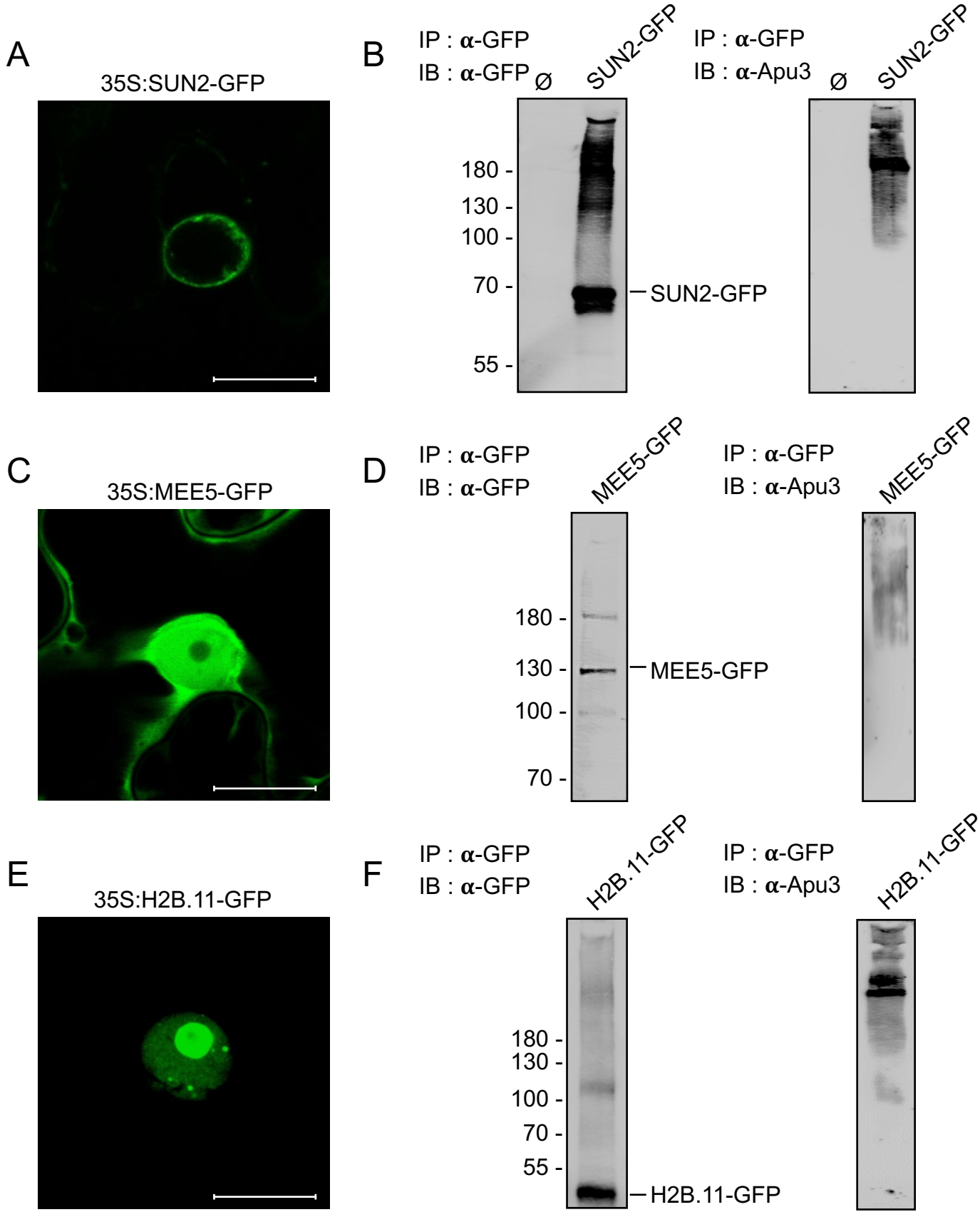

Figure 8. Validation of K63 polyubiquitination for nuclear hits identified by sensor-based proteomics using transient expression in wild tobacco. A, C, E, Subcellular localization of SUN2-GFP (A), MEE5-GFP (C), and H2B.11-GFP (E) transiently expressed in *Nicotiana benthamiana* leaves. Scale bars = 10 µm. B, D, F, *In vivo* K63 polyubiquitination of transiently expressed SUN2 (B), MEE5-GFP (D), and H2B.11-GFP (F). Immunoprecipitation was performed using anti-GFP antibodies on RIPA buffer-solubilized protein extracts. *Nicotiana benthamiana* plants expressing free GFP were used as a negative control (0). Eluates were subjected to immunoblotting with anti-GFP and anti-K63 polyUb antibodies (Apu3). IB, immunoblotting, IP, immunoprecipitation. The sizes of marker proteins in kDa are shown.